The human glucocorticoid receptor variant rs6190 promotes blood cholesterol and atherosclerosis

Authors:

Hima Bindu Durumutla[1,2], April Haller[3], Greta Noble[1], Ashok Daniel Prabakaran[1], Kevin McFarland[1], Hannah Latimer[1], Olukunle Akinborewa[1,4], Bahram Namjou-Khales[2,4], David Y. Hui[2], Mattia Quattrocelli[1*]

Affiliations:

[1]Molecular Cardiovascular Biology, Heart Institute, Cincinnati Children's Hospital Medical Center, Cincinnati, OH, USA.

[2]Dept. Pediatrics; [3]Department of Pathology; [4] Dept Pharmacology, Physiology and Neurobiology; University of Cincinnati College of Medicine, Cincinnati, OH, USA.

[4]Center for Autoimmune Genomics and Etiology, Cincinnati Children's Hospital Medical Center, Cincinnati, OH, USA.

***Corresponding Author:**

Mattia Quattrocelli, PhD, Molecular Cardiovascular Biology, Heart Institute, Cincinnati Children's Hospital Medical Center, 240 Albert Sabin Way T4.676, Cincinnati, OH 45229. Email: mattia.quattrocelli@cchmc.org, tel: +1-513-517-1221

Keywords – Rs6190, ER22/23K, glucocorticoid receptor, SNP, cholesterol, atherosclerosis, liver, hiPSCs, hepatocytes, LDL receptor, PCSK9, transactivation.

Word count (including title page, full text, references, figure legends) – 10,266 words.

Data availability – RNA-seq and ChIP-seq datasets reported here are available on GEO as GSE280494 and GSE280572.

Author contributions –HBD, AH, GN, ADP, KMF, HL, OA, BNK: Data curation, Formal analysis, Investigation; AJ, DYH: Resources; MQ: Conceptualization, Formal analysis, Funding acquisition, Supervision.

Conflicts of Interest – MQ is listed as co-inventor on a patent application related to intermittent glucocorticoid use filed by Northwestern University (PCT/US2019/068,618), unrelated to any aspects of this study. All other authors declare they have no competing interests.

Graphical Abstract

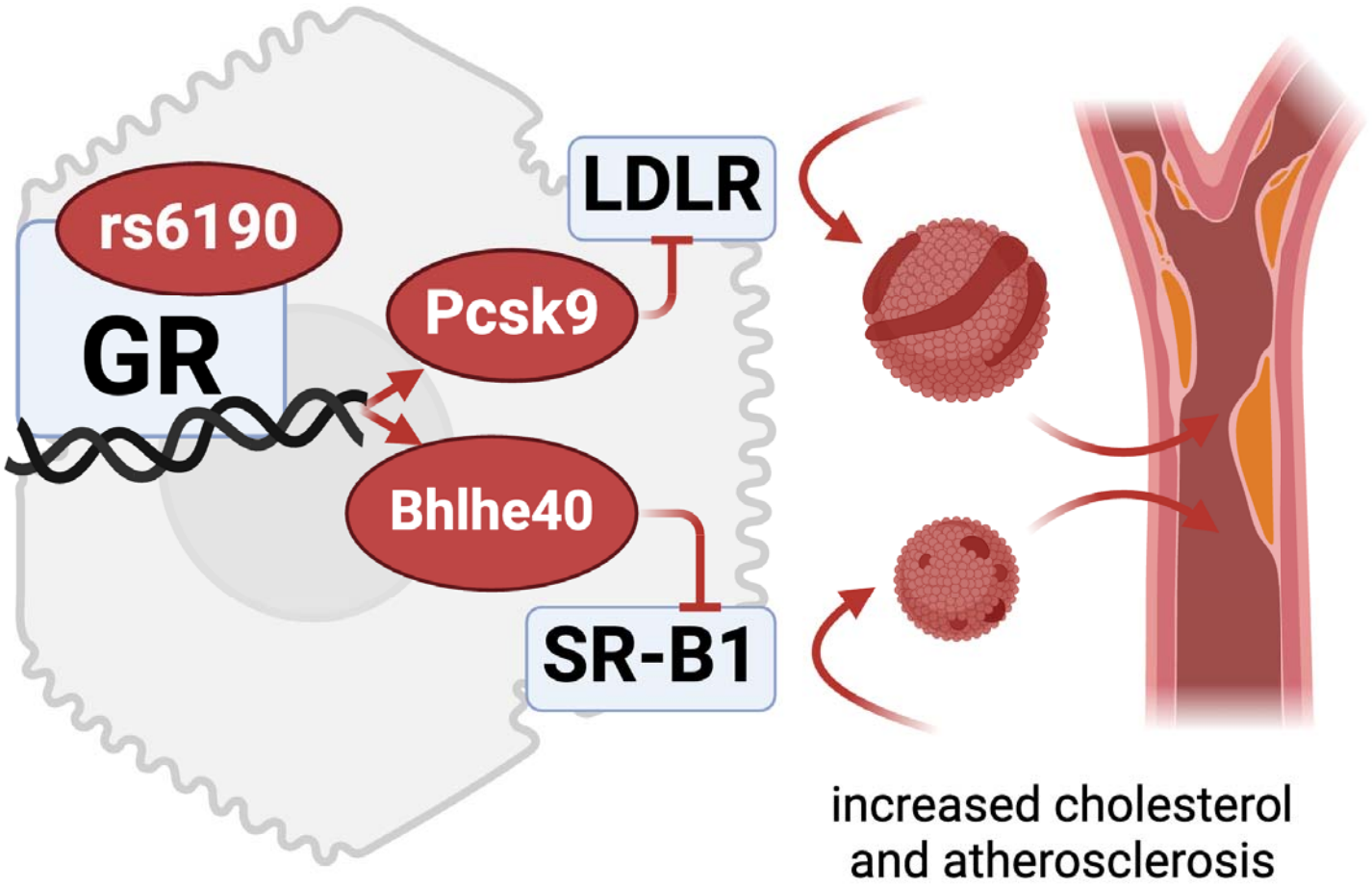

Abstract

Elevated cholesterol poses a significant cardiovascular risk, particularly in older women. The glucocorticoid receptor (GR), a crucial nuclear transcription factor that regulates the metabolism of virtually all major nutrients, harbors a still undefined role in cholesterol regulation. Here, we report that a coding single nucleotide polymorphism (SNP) in the gene encoding the GR, *rs6190*, associated with increased cholesterol levels in women according to UK Biobank and All Of Us datasets. In SNP-genocopying transgenic mice, we found that the rs6190 SNP enhanced hepatic GR activity to transactivate *Pcsk9* and *Bhlhe40*, negative regulators of low-density lipoprotein (LDL) and high-density lipoprotein (HDL) receptors in liver respectively. Accordingly, in mice the rs6190 SNP was sufficient to elevate circulating cholesterol levels across all lipoprotein fractions and the risk and severity of atherosclerotic lesions on the pro-atherogenic *hAPOE*2/*2* background. The SNP effect on atherosclerosis was blocked by in vivo knockdown of Pcsk9 and Bhlhe40 in liver. Remarkably, we found that this mechanism was conserved in human hepatocyte-like cells using CRISPR-engineered, SNP-genocopying human induced pluripotent stem cells (hiPSCs). Taken together, our study leverages a non-rare human variant to uncover a novel GR-dependent mechanism contributing to atherogenic risk, particularly in women.

Introduction

Hypercholesterolemia, i.e. elevated plasma cholesterol, is a major risk factor for atherosclerotic cardiovascular disease, particularly in older women (1, 2). Although advancements in drug therapies and lifestyle interventions have demonstrated efficacy, the identification of genetic and epigenetic factors regulating cholesterol is still ongoing to increase our mechanistic understanding and better predict and manage hypercholesterolemia.

Despite its involvement in virtually every nutrient metabolism, the glucocorticoid receptor (GR) remains a poorly defined nuclear factor in cholesterol homeostasis. The GR is a ligand-activated nuclear transcription factor that exerts multifaceted effects on nutrient metabolism (3, 4) by transactivating or transrepressing large gene programs in a tissue-specific manner (5). While traditionally recognized for its role in immune regulation, GR profoundly influences metabolic processes, including glucose and lipid metabolism (6). Prior studies employing GR knockdown in liver and adipose tissue have shown promising outcomes in mitigating hypercholesterolemia and associated metabolic abnormalities in obese diabetic mice (7). Retrospective studies involving pathomorphological data obtained from human autopsies have provided insights into potential relationships between glucocorticoid treatments and atherogenesis (8-11). However, the direct link between the hepatic GR and regulation of cholesterol levels remains elusive. Indeed, although the glucocorticoid-GR axis has been implicated in apolipoprotein expression (12) and cholesterol efflux in macrophages (13, 14), the epigenetic and transcriptional mechanisms enabled by the GR in hepatocyte-autonomous cholesterol uptake remain still poorly defined.

Previously, several genetic variants in the GR gene (*NR3C1;* OMIM #138040) have been described in the human population. These genetic variants can affect the transcriptional activity of the GR and its downstream target genes, potentially influencing nutrient regulation (15-18). Epidemiological studies have provided evidence of an association between specific GR polymorphisms and variation in lipid profiles (15, 19, 20). Notably, the *rs6190* (c.68G>A; p.R23K) coding single nucleotide polymorphisms (SNP) - also known as “E22R/E23K” due its complete linkage to the silent p.E22E *rs6189* SNP - is a missense mutation at codon 23 in the N-terminus of the GR protein, resulting in an amino acid change from arginine (R) to lysine (K) (21). This mutation has been linked to alterations in several parameters of metabolic homeostasis in humans, including cholesterol (17). However, the precise molecular mechanisms through which this polymorphism skews GR activity to perturb cholesterol remain poorly characterized.

In this study, we harnessed the human *rs6190* SNP to identify a direct GR-mediated program governing hepatic cholesterol regulation and its association with atherogenic risk. We found that this low-frequency coding SNP correlated with increased levels of cholesterol in women from UK Biobank and All of Us cohorts, and promoted cholesterol and atherosclerosis in transgenic mice according to the number of SNP alleles (homo>hetero>reference). Our transcriptomic and epigenetic datasets revealed that the mutant GR perturbed cholesterol levels through transactivation of *Pcsk9* and *Bhlhe40*, negative regulators of LDL and HDL receptors in the liver and previously unknown targets of GR. Our study identifies rs6190 as a potential risk factor for ath-

erosclerosis, particularly in women, and reports unanticipated mechanisms through which the hepatic GR impacts cholesterol levels in the circulation.

Results

rs6190 SNP increases plasma cholesterol levels in women according to allele zygosity.

To investigate the influence of rs6190 variant on cholesterol regulation, we probed the large adult cohort from the United Kingdom (UK) Biobank, comprising of 485,895 at the age of 40-70 years. In this cohort, the GR rs6190 variant (*NR3C1* gene, transcript ENST00000231509.3 (-strand); c.68G>A; p.R23K) exhibited a minor allele frequency of 2.75% (25,944 heterozygous, 413 homozygous individuals), categorizing it as a low-frequency variant (21). We screened the quantitated parameters from the NMR metabolomics dataset within the UK Biobank dataset (120,356 individuals comprising of 65156 women and 55380 men; same age range as general dataset, 40-70 years) for rs6190 associations disaggregated by sex. All analyses were adjusted for age, body mass index (BMI), top 10 principal components, and genotype information for 12 commonly-referenced, hypercholesterolemia-associated SNPs within *PCSK9, CELSR2, APOB, ABCG8, SLC22A1, HFE, MYLIP, ST3GAL4, NYNRIN, LDLR,* and *APOE* genes (22). Importantly, none of these 12 classical variants were in the neighborhood of rs6190 and did not show significant pairwise LD (linkage disequilibrium) effect (r^2 < 0.001) at the genomic level. While no associations were significant after multiple testing in men, rs6190 SNP significantly associated with many cholesterol parameters in women, accounting for 23 out of 33 total plasma parameters with a significant rs6190 effect (adjusted p<0.005) (**Figure 1A**).

We then stratified total, LDL-, and HDL-cholesterol values from women according to SNP zygosity. We are defining here homozygous carriers of the reference allele (control population) as $GR^{ref/ref}$, heterozygous SNP carriers as $GR^{ref/ALT}$, and homozygous SNP carriers as $GR^{ALT/ALT}$. We performed linear regressions with a mixed model correcting for age, BMI, diabetic status and triacylglycerols. In parallel, we also compared median confidence intervals across rs6190 genotypes. Remarkably, total, LDL-, and HDL-cholesterol showed a modest but significant elevation of median levels according to the number of SNP alleles in women (**Figure 1B**). The zygosity-dependent trends were not significant in men **(Suppl. Fig. 1A)**. Considering the effects on cholesterol, we probed the total UK Biobank dataset for hypercholesterolemia and cardiovascular disease mortality odds ratios. In alignment with the trends in cholesterol, $GR^{ALT/ALT}$ women displayed an increased odds ratio of 1.34 (95% CI: 1.02 – 1.76; P=0.0092) for hypercholesterolemia (total cholesterol >240 mg/dl) and 2.37 (95% CI: 1.05 – 5.9; P=0.01) for death due to cardiovascular diseases, compared to $GR^{ref/ref}$ women (**Figure 1C-D**).

To probe these rs6190 correlations in a more genetically diverse human dataset, we queried the All Of Us dataset, where we found the SNP at a variable minor allele frequency ranging from low-frequency to rare across ancestries: African/African-American, 0.49%; American Admixed/Latino, 0.84%; East Asian, 0.061%; European, 2.67%; Middle Eastern, 1.43%; South Asian, 1.49%. In the All Of Us subset of 245,385 individuals with rs6190 genotype annotation encompassing all ancestries and ages, we repeated the linear regressions corrected for age, BMI, diabetes, triacylglycerols, as well as the median comparisons. The analyses in the All of Us dataset confirmed a significant correlation between rs6190 zygosity and total, LDL and HDL cholesterol levels in women **(Figure 1E)**, while correlations were not significant once again in men **(Suppl. Fig. 1B)**.

Taken together, our findings highlight the association of the rs6190 SNP with modest but significant and potentially consequential elevations of cholesterol in women from the UK Biobank and the All Of Us cohorts.

The rs6190 SNP is sufficient to increase plasma cholesterol and promotes GR transactivation of Pcsk9 and Bhlhe40 in mice.

To elucidate the extent to which the mutant GR promotes cholesterol elevation, we introduced a genocopy of the rs6190 SNP into the endogenous *Nr3c1* (GR gene) locus on the C57BL/6J background. The murine ortholog of the human GR-R23K mutation is GR-R24K due to an additional amino acid in position 10. Employing CRISPR-mediated knock-in recombination, the murine GR gene was targeted at the orthologous codon 24 resulting in C>T mutation in the forward strand (c.71G>A mutation in the codon, reverse strand) leading to a p.R24K amino acid substitution (**Suppl. Figure 2A**). In concordance with human carriers, we define here homozygous mice for wild-type allele as "$GR^{re/ref}$" (control), heterozygous SNP mice as "$GR^{ref/ALT}$", and homozygous SNP mice as "$GR^{ALT/ALT}$". In female littermate mice under normal chow conditions, total plasma cholesterol increased according to SNP zygosity in both fasted and fed states (**Figure 2A**). Using the standard fast-performance liquid chromatography (FPLC) method, we found that the GR SNP elicited an increase in cholesterol levels across all lipoprotein fractions – VLDL-, LDL- and HDL-cholesterol - according to SNP allele number, in conditions of either regular chow or 16-week long Western diet in female (**Figure 2B**), but not male mice **(Suppl. Fig. 2B)**. This sex-specific effect in mice paralleled the correlations within human datasets and prompted us to focus on female mice for the bulk of our histological, physiological and mechanistic analyses. After Western diet exposure, in 3 out of 5 analyzed $GR^{ALT/ALT}$ female mice, we found histological evidence of immature plaque formation in the aortic root (**Suppl. Fig. 2C**), a remarkable finding in the absence of pro-atherogenic genetic backgrounds. Moreover, considering that the GR naturally responds to diurnal oscillations in endogenous glucocorticoids (corticosterone in mice), we followed the circadian oscillations in cholesterol across genotypes. The SNP effect on cholesterol elevation was significant through the circadian cycle and particularly acute during the dark phase (corticosterone peak in mice), without significant changes in corticosterone levels per se (**Suppl. Fig. 2D**). Our findings provide evidence that, in homogeneous genetic settings, the SNP is sufficient to modestly but significantly elevate total, LDL-, and HDL-cholesterol in females according to an incomplete dominance model, i.e. commensurate to SNP zygosity.

We then focused our mechanistic analyses on $GR^{ref/ref}$ vs $GR^{ALT/ALT}$ liver comparisons, considering the primary role of this organ in cholesterol regulation (23). In primary hepatocytes, the mutant GR showed an increased epigenetic activity both at baseline and after glucocorticoid stimulation, assayed through a luciferase reporter (**Suppl. Fig. 2E**). We therefore conducted RNA-sequencing and GR ChIP-sequencing in liver to identify potential differential targets of GR transactivation based on GR SNP genotype. The liver GR ChIP-seq was validated by enrichment for the canonical GRE motif in unbiased motif analysis (**Suppl. Figure 2F**). Compared to the control GR, the increased epigenomic activity of the mutant GR was evidenced by increased GR signal on GRE sites genome-wide and on the *Fkbp5* promoter, a canonical marker for GR activity (24, 25) (**Suppl. Fig.**

2G-H). No statistical differences were noted in overall peak number or genomic peak distribution, which clustered preferentially in proximal promoter regions for both genotypes (**Suppl. Fig. 2I-J**). Liver RNA-seq revealed 368 genes with differential expression by the mutant GR (**Suppl. Fig. 2K**). The overlay of both datasets unveiled 236 genes exhibiting both differential expression and a gain of mutant GR signal on their promoters (**Figure 2C**). Gene ontology (GO) analysis revealed a significant enrichment for cholesterol metabolism. Notably, within this pathway, proprotein convertase subtilisin/kexin type 9 (*Pcsk9*) was the highest hit. The increased transactivation of *Pcsk9* in liver by the mutant GR was validated at mRNA and protein levels (**Figure 2D-E**). Besides indirect and direct inhibition of VLDL-cholesterol clearance (26, 27), PCSK9 plays a pivotal role in increasing circulating LDL cholesterol by promoting the degradation of the main LDL-cholesterol receptor, LDLR, at the protein level (28, 29). Accordingly, the gain in PCSK9 levels correlated with a reduction in protein but not mRNA levels of LDLR in $GR^{ALT/ALT}$ compared to $GR^{ref/ref}$ liver tissues (**Figure 2D-E**). Additionally, within the "rhythmic process" pathway from the ChIP-seq/RNA-seq overlay, the top hit for mutant GR transactivation was *Bhlhe40* (**Figure 2C**), a transcriptional repressor involved in many processes including circadian clock homeostasis (30, 31). Using an ENCODE-mining platform for transcription factor target prediction (32), we screened for putative *Bhlhe40* targets in the promoters of down-regulated genes in mutant versus WT livers. This analysis revealed Scavenger Receptor Class B Type I (SR-B1), encoded by *Scarb1*, as a unique hypothetical target of BHLHE40 from our RNA-seq datasets. SR-B1 is the main receptor for reverse HDL-cholesterol transport in the liver (33). Consistent with our prediction, *Bhlhe40* upregulation correlated with SR-B1 downregulation at both mRNA and protein levels in $GR^{ALT/ALT}$ compared to $GR^{ref/ref}$ liver tissues (**Figure 2D-E**). Additionally, to confirm the in-silico prediction of SR-B1 transcriptional repression by BHLHE40, we compared *Scarb1* expression and SR-B1 protein levels in liver tissues from *Bhlhe40*$^{null/null}$ (34) *(Bhlhe40-KO*) vs their wild-type littermate controls (*Bhlhe40-WT*). As hypothesized, SR-B1 was upregulated in the *Bhlhe40-KO* livers compared to WT controls (**Suppl. Fig. 2L**). We then asked the extent to which the mutant GR effect on LDLR and SR-B1 downregulation was biologically significant on hepatocyte biology. We probed fluorescently-labeled LDL and HDL uptake assays in primary hepatocytes to assess this propensity in the absence of body-wide confounders. In line with the LDLR and SR-B1 changes, the $GR^{ALT/ALT}$ hepatocytes showed decreased LDL and HDL uptake *in vitro* compared to $GR^{ref/ref}$ control hepatocytes (**Figure 2H**). Collectively, our findings support a mechanism for the rs6190 SNP effect on cholesterol through which the SNP skews the hepatic GR epigenetic activity and promotes transactivation of *Pcsk9* and *Bhlhe40*, which in turn decreases LDL and HDL cholesterol uptake in liver by repressing LDLR and SR-B1 levels respectively.

CRISPR-engineered hiPSC-derived hepatocytes confirm the mouse-to-human relevance for the SNP mechanism.

In tandem with our murine mouse studies, we questioned whether the molecular SNP mechanism identified was translatable to human hepatocytes. We, therefore, generated SNP heterozygous and homozygous lines from the same parental $GR^{ref/ref}$ hiPSC line through a CRISPR-knockin system. Individual founding clones of

isogenic $GR^{ref/ref}$ (control), $GR^{ref/ALT}$ (het), and $GR^{ALT/ALT}$ (homo) hiPSCs were verified through Sanger sequencing and quality-controlled for pluripotency marker expression (**Figure 3A; Suppl. Fig. 3A**). Despite no differences in pluripotency markers, the SNP significantly skewed the GR to a higher rate of glucocorticoid-driven GR translocation in hiPSCs, as shown by serial imaging after a dexamethasone pulse (**Suppl. Fig. 3B**) and consistent with our previous findings with the mutant GR in murine hepatocytes luciferase assay and liver ChIP-seq.

To investigate whether the SNP-mediated molecular mechanism was conserved in human hepatocytes, we subjected the isogenic lines of hiPSCs to a 23-day differentiation protocol to generate mature hepatocyte-like cells (HLCs) (35). Given the well-established role of GR as a regulator of hepatocyte differentiation and maturation (36-38), we sought to investigate whether the presence of the GR SNP influenced the differentiation process. To address this, we examined the expression profiles of differentiation markers at multiple time points during the differentiation process: *NANOG* and *OCT4* at the pluripotent stage (39); *SOX17* and *FOXA2* at the definitive endoderm stage (40); *AFP* and *HNF1A* at the immature hepatocyte stage (41); *ALB* and *CY18*, morphology, and albumin secretion at the mature hepatocyte stage (42). We did not detect any SNP-driven significant alterations in the *in vitro* maturation process of hiPSC-derived hepatocytes (**Suppl. Fig. 3C-D**). However, the hiPSC-derived hepatocytes reproduced the zygosity-dependent increase in GR nuclear translocation (**Figure 3B**) and the SNP-mediated effects on *PCSK9* and *BHLHE40* transactivation, as well as post-translational repression of LDLR and SR-B1 (**Figure 3C**). Furthermore, the $GR^{ALT/ALT}$ hiPSC-derived hepatocytes displayed decreased uptake of HDL and LDL-cholesterol compared to $GR^{ref/ref}$ control cells (**Figure 3D-E**). Taken together, our hiPSC-derived hepatocyte data confirm that the molecular SNP mechanism is conserved in human cells and appears autonomous to hepatocytes in the absence of *in vivo* body-wide physiology.

rs6190 GR SNP promotes atherosclerosis in vivo.

Despite our results so far linking the mutant GR to cholesterol regulation, the extent to which the overall SNP-enabled program significantly impacts atherosclerosis *in vivo* remains unknown. To evaluate the extent to which the rs6190 SNP contributes to atherogenic risk *in vivo* in conditions of genetic homogeneity, we crossed our mutant SNP mice with the atherogenic background characterized by homozygous expression of the human *APOE*2* variant (43, 44). The h*APOE*2/*2* mice are well-established transgenic mice known for their susceptibility to atherosclerosis while maintaining cholesterol distribution across all three major lipoprotein compartments (44, 45), unlike other atherogenic backgrounds like *ApoE-KO*. We also excluded the *Ldlr-KO* background as a direct genetic confounder of our LDLR-involving hypothesis.

For these analyses, we focused on $GR^{ALT/ALT}$ vs $GR^{ref/ref}$ female mice. On the h*APOE*2/*2* background and regular chow diet, $GR^{ALT/ALT}$ mice exhibited elevated levels of VLDL-, LDL- and HDL-cholesterol in the FPLC curves compared to control littermates, and this was reinforced even more after a 16-week-long Western diet exposure (**Figure 4A**). We focused on mice exposed to Western diet for atherosclerotic plaque analyses.

Compared to $GR^{ref/ref}$, $GR^{ALT/ALT}$ mice exhibited a significant increase in atherosclerotic plaque incidence as quantitated through overall plaque/total aorta area ratio in en face whole aorta staining and imaging (**Figure 4B, left**). Furthermore, histological analysis of the aortic root cross-sections and Oil Red O staining revealed a significant increase in atherosclerotic lesion size (plaque/lumen ratio) and lipid accumulation in $GR^{ALT/ALT}$ versus $GR^{ref/ref}$ mice (**Figure 4B, right**). Finally, considering our hypothesis of *Pcsk9* and *Bhlhe40* as mechanistic mediators of the SNP effect, we tested the effect of *in vivo* knock-down of these genes on the SNP-mediated effect on cholesterol and atherosclerosis through AAV8 vectors. For *Pcsk9* knockdown we used a previously reported AAV vector (46) and confirmed its max knockdown effect in liver in vivo in Apo*2/*2 mice on Western Diet with a 10^13vg/mouse dose **(Suppl. Fig. 4A)**. For *Bhlhe40*, we combined two AAVs with different shRNAs under the U6 promoter, as they showed synergistic effect on *Bhlhe40* knockdown in Apo*2/*2 livers **(Suppl. Fig. 4B)**. At 2 months of age, $GR^{ALT/ALT}$ vs $GR^{ref/ref}$ female mice on the ApoE*2/*2 background were injected retro-orbitally (r.o.) with $3x10^{13}$ vg/mouse AAV-scramble or 10^{12} vg/mouse/vector AAV-antiPcsk9 (1 vector) + AAV-antiBhlhe40 (2 vectors) immediately before starting the 16-week-long Western Diet exposure. At endpoint, we validated target gene knockdown **(Fig. 4C)** and we focused on FPLC cholesterol curves and atherosclerotic plaques as read-outs. Compared to scramble, the knockdown vectors reduced the cholesterol levels across lipoprotein fractions in $GR^{ALT/ALT}$ mice to $GR^{ref/ref}$-like levels **(Fig. 4D)**, and blunted the SNP-mediated effect on plaque incidence (**Fig. 4E**) and severity **(Fig. 4F)**. We also noted that the knockdown vectors reduced VLDL-cholesterol and plaque incidence but not histological plaque severity in $GR^{ref/ref}$ mice compared to scramble. Taken together, our findings demonstrate that the rs6190 SNP promotes hypercholesterolemia and atherosclerosis *in vivo* through upregulation of *Pcsk9* and *Bhlhe40* in liver.

Discussion

The glucocorticoid receptor (GR) is well-known for its involvement in orchestrating large gene programs and modulating hepatic lipid and glucose metabolism. However, the precise mechanisms by which hepatic GR governs cholesterol regulation remains elusive. Despite the well-established association between chronic glucocorticoid exposure and hypercholesterolemia with concomitant metabolic stress (47), a direct link between GR and atherosclerosis remains unclear. In this study, we leveraged a naturally occurring human mutation, the rs6190 SNP, to unveil a direct GR-mediated program governing hepatic cholesterol regulation and its consequential implication for atherogenic risk. We focused here on the hepatic transactivation targets of the mutant GR based on ChIP-seq-RNA-seq overlay, and consequently validated *Pcsk9* and *Bhlhe40* as mediators of the SNP effect on LDLR and SR-B1 levels in liver, as well as on overall cholesterol levels and atherosclerosis in the *hAPOE*2/*2* background. We recognize that our study did not address potential mutant GR effects on apolipoproteins (e.g. ApoE itself) or macrophages, both critical determinants of atherosclerosis and in turn regulated by glucocorticoids and/or GR (12, 13). While beyond the focus of the present study, these are compelling questions to address to expand significance of our findings for overall hypercholesterolemia and atherosclerosis risk in SNP carriers.

Our mixed-model regressions in the UK Biobank and the All Of Us datasets have unveiled an unexpected association between the rs6190 SNP and elevated levels of total, LDL-, and HDL-cholesterol in women. Importantly, the impact of the rs6190 genetic variant demonstrated an additive effect based on SNP zygosity, i.e. according to the number of “risk” alleles. Additionally in the UK Biobank, the rs6190 SNP correlated with increased odds ratio for hypercholesterolemia and cardiovascular-related mortality. It was compelling to find analogous correlations in two cohorts that are quite different with regards to genetic ancestry composition. In the All Of Us cohort, the highest minor allele frequency for the SNP was in individuals with European ancestry and closely matched the minor allele frequency of the UK Biobank, where the “white British ancestry” indeed accounts for almost 90% of the cohort (48). Beyond SNP correlations in human datasets, we sought to gain the mechanistic insight in mice and hiPSCs of the extent to which the rs6190 SNP is sufficient to regulate cholesterol. Our findings in murine liver and hiPSC-derived hepatocytes show the SNP is indeed sufficient to elevate cholesterol and promote atherosclerosis through a specific change in the GR activity. In principle, this is a novel mechanism of SNP action that is independent from the genomic context. Future studies will be needed to articulate the genetic modifiers that potentiate or contrast this mechanism across ancestries in the human population.

Given the well-established role of GR as a potent transcription factor, we examined the potential alterations in the epigenetic activity of GR induced by the rs6190 mutation. At the molecular level, our findings revealed that the mutant GR exhibited increased epigenetic activity and nuclear translocation, leading to the differential expression of 236 genes, including key regulators of cholesterol metabolism. Notably, the mutant GR upregulated *Pcsk9*, a key regulator of VLDLR and LDLR degradation, and *Bhlhe40*, a circadian transcriptional repressor that is implicated in SR-B1 control. At present, additional experiments are required to ascertain the extent to

which the increase in cholesterol is independent of general changes in lipidemia. However, we emphasize that our regression analyses in women from the UK Biobank dataset took into account triacylglycerols as co-variate, and still found a significant zygosity-dependent effect on total and LDL-cholesterol.

To confirm the conservation of the SNP-mediated mechanism, we utilized isogenic hiPSC-derived hepatocytes carrying the rs6190 SNP. These hiPSC-derived hepatocytes exhibited increased expression of *PCSK9* and *BHLHE40*, consistent with murine model findings. Moreover, these hepatocytes demonstrated reduced uptake of HDL and LDL cholesterol, providing direct evidence that the SNP influences cholesterol regulation and this mechanism is conserved in human cells. Although the rs6190 SNP is described in ClinVar as associated with "glucocorticoid resistance," our analyses in hiPSCs and hiPSC-derived hepatocytes revealed that the mutant GR is more susceptible to glucocorticoid-induced activation than the reference GR isoform. This observation suggests that the SNP may confer increased "glucocorticoid sensitivity" in addition to its effects on cholesterol regulation. The evidence in support of "glucocorticoid resistance" is mostly limited to one study, where targeted limited analyses found that rs6190 decreased dexamethasone-driven activation of *GILZa* in immune cells (49). However, several subsequent studies have failed to find correlation between rs6190 and reduced sensitivity to glucocorticoids, including the seminal study that first discovered the rs6190 polymorphism (21, 24, 47, 50-53). Further *in vitro* experiments are warranted to investigate the extent to which the mutant GR activates newly identified glucocorticoid response elements (GREs) dependently or independently from other key nuclear factors for cholesterol regulation.

Limitations of this study – Besides specific limitations and considerations reported above for specific results, in this study we have not formally assessed the impact of sexual dimorphism on the SNP effect. While a previous study in a limited cohort found a significant association between the rs6190 SNP and lower cholesterol levels in men but not in women (17), our investigations in the large UK Biobank and All Of Us cohorts revealed a significant association between the SNP and increased cholesterol levels in women but not in men. Our studies in SNP mice further confirmed a significant or larger magnitude of SNP effect in female rather than male mice. These sex-specific observations will require well-powered studies to disentangle the interplay between the mutant GR and sex-specific nuclear receptor cascades from the sexual dimorphism in downstream cholesterol regulations, complex experiments that go beyond the mechanistic discovery focus of this initial study.

Conclusions and overall impact – In conclusion, our study leverages the rs6190 SNP as genetic linchpin to advance our understanding of the GR-driven regulation of cholesterol through genetic and epigenetic mechanisms. Our data support early and proactive monitoring for cholesterol in carriers of this non-rare variant, particularly in women.

Figure 1

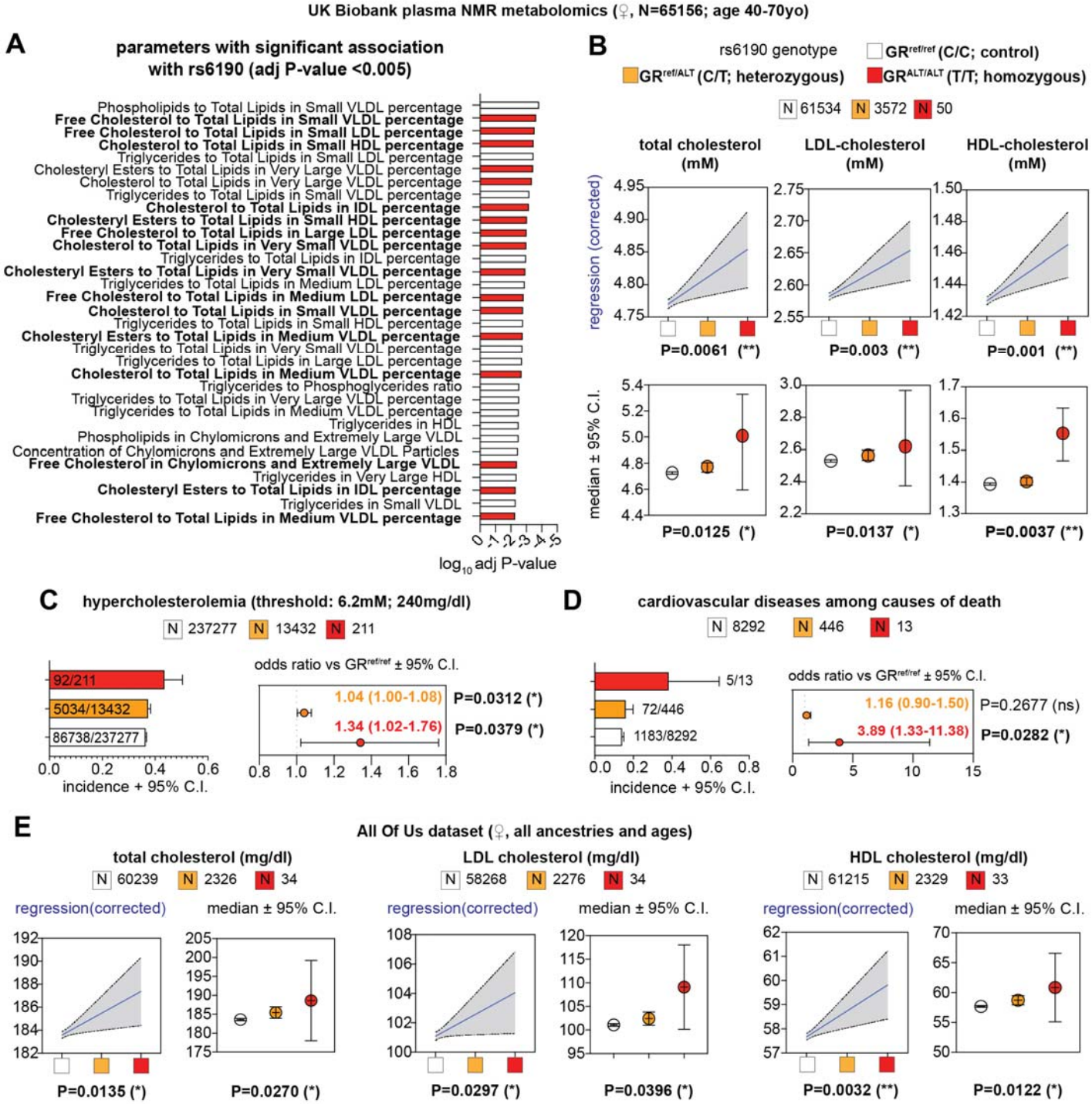

Figure 1 – rs6190 correlates with cholesterol increase in women from the UK Biobank and All of US datasets. (A) Unbiased ranking of UK Biobank plasma NMR parameters for significant rs6190 effect in women. Cholesterol-related parameters are highlighted in bold text and red bars. P values were adjusted for age, BMI and canonical hypercholesterolemia-associated SNPs. **(B)** Linear regressions (blue lines; shaded area represents 95% C.I.; corrected for age, diabetes, triacylglycerols) and median confidence intervals (Kruskal-Wallis test) show zygosity-dependent trends in elevation of total, LDL- and HDL-cholesterol in women. **(C-D)** Compared to non-carriers, homozygous SNP carriers showed increased odds ratio for hypercholesterolemia and cardiovascular disease deaths according to ICD10 codes; Chi-square test. **(E)** Linear regressions and median comparisons correlated rs6190 genotype with cholesterol elevation in women from the All of Us dataset, including all ancestries and ages. *, P<0.05; **, P<0.01; ***, P<0.001; ****, P<0.0001.

Figure 2

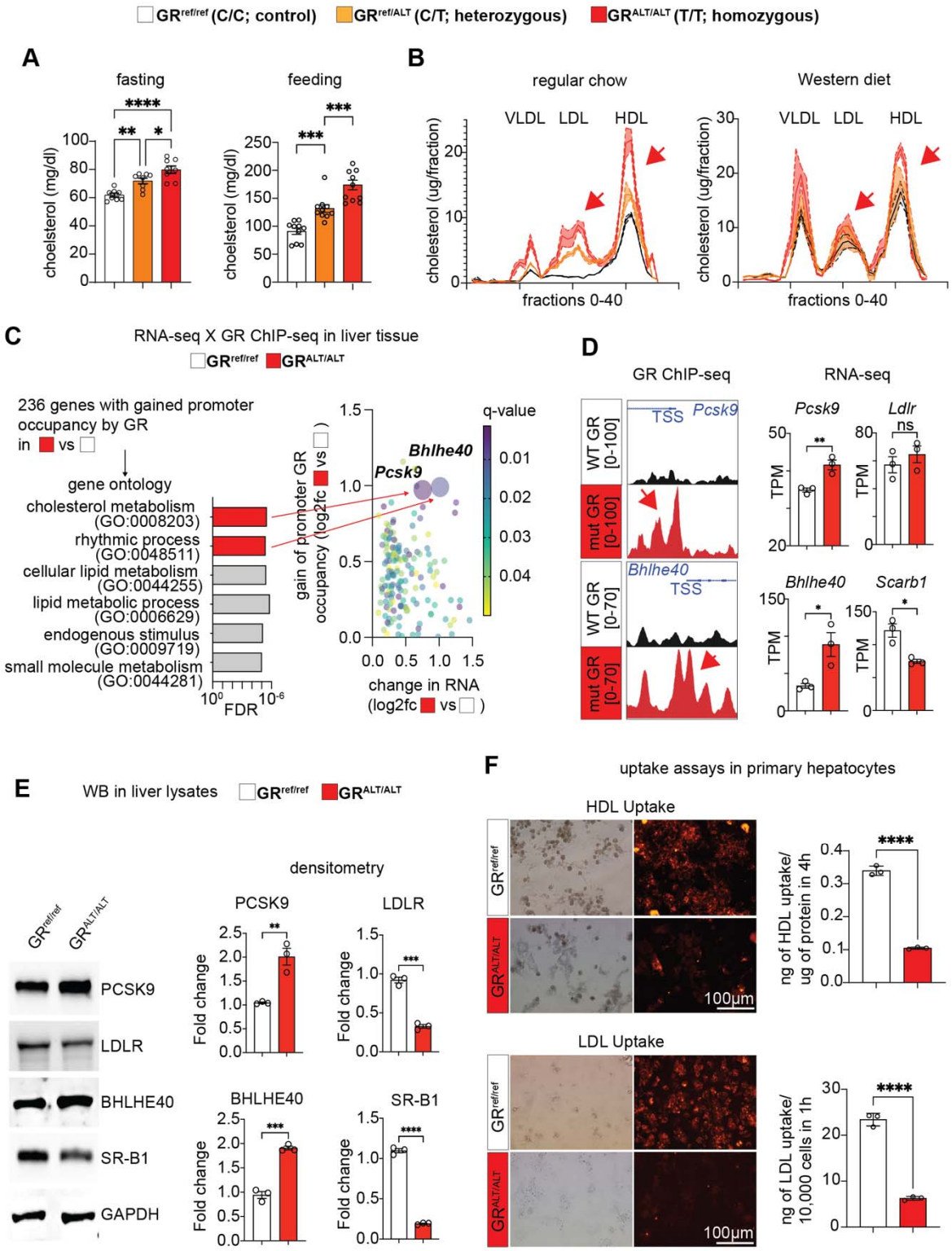

Figure 2. The rs6190 SNP is sufficient to increase cholesterol and skew the liver GR to a gene program repressing liver cholesterol uptake in mice. (A) Zygosity-dependent increases in cholesterol in both fed and fasted states in littermates control vs SNP-carrier mice. **(B)** Analogous trends with regular and Western diets, as assayed through FPLC distribution of cholesterol across lipoprotein fractions (arrows highlight increases in LDL- and HDL-cholesterol). **(C)** RNA-seq and ChIP-seq overlay in liver tissue identifies *Pcks9* and *Bhlhe40* as putative transactivation targets of the mutant GR. **(D-E)** ChIP-seq and RNA-seq, as well as validation WB values for PCSK9, BHLHE40 and their putative targets LDLR and SR-B1. **(F)** Uptake of LDL and HDL particles (traced by red fluorescence) is lower in $GR^{ALT/ALT}$ than $GR^{ref/ref}$ primary hepatocytes. N=3-10♀/group, 3-6mo; A: 1w ANOVA + Sidak; D-F: Welch's t-test; *, P<0.05; **, P<0.01; ***, P<0.001; ****, P<0.0001.

Figure 3

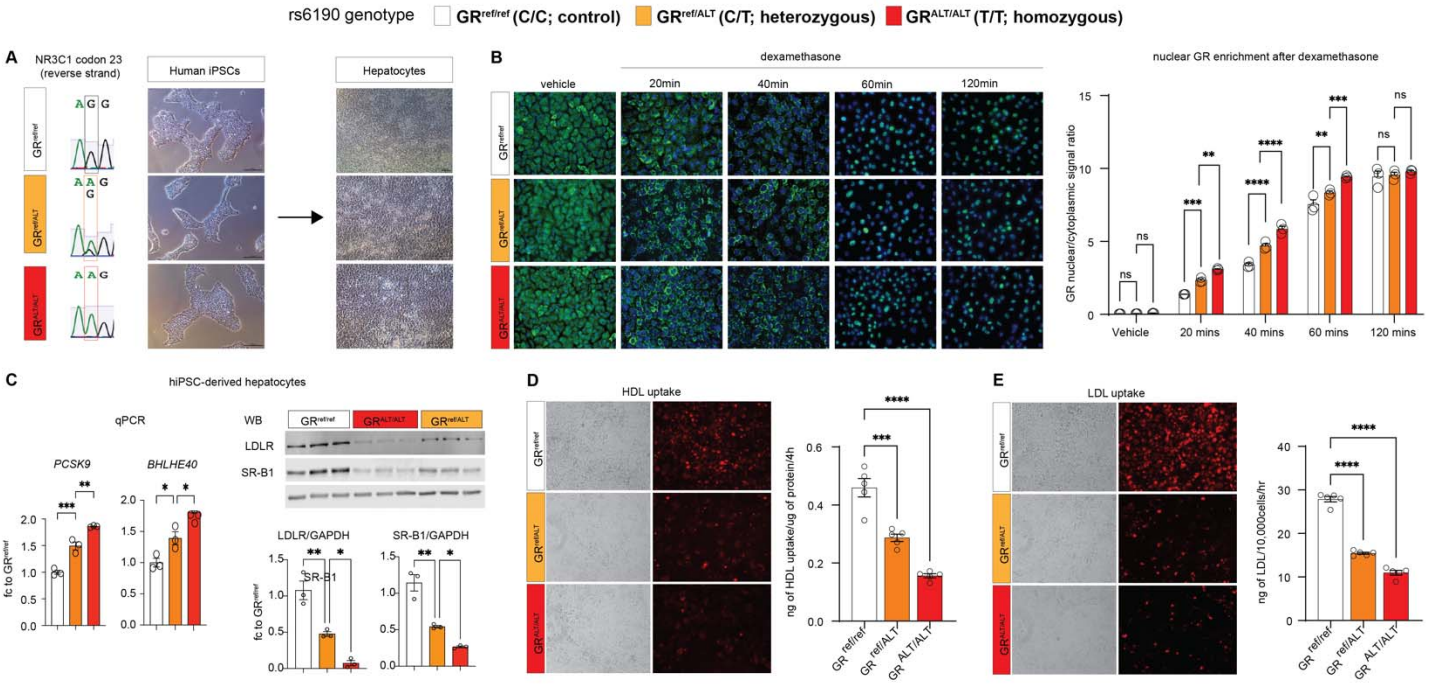

Figure 3. The SNP molecular effects are replicated in hiPSC-derived hepatocytes. (A) Sanger sequencing of SNP genotype and brightfield representative images for isogenic hiPSCs and derived hepatocytes with no, one or two rs6190 SNP alleles. **(B)** Rate of GR nuclear signal enrichment in hiPSC-hepatocytes increased between 20-60min after dexamethasone addition according to SNP zygosity. **(C)** Zygosity-dependent effects on *PCSK9* and *BHLHE40* upregulation at the hepatocyte level, as well as on protein level downregulation for LDLR and SR-B1. **(D-E)** SNP zygosity replicated the effects on HDL and LDL fluorescent particle uptake in hiPSC-hepatocytes. Each dot represents an independent differentiation replicate; N=3-6/group. B: 2w ANOVA + Sidak; C-E: 1w ANOVA + Sidak. *, P<0.05; **, P<0.01; ***, P<0.001; ****, P<0.0001.

Figure 4

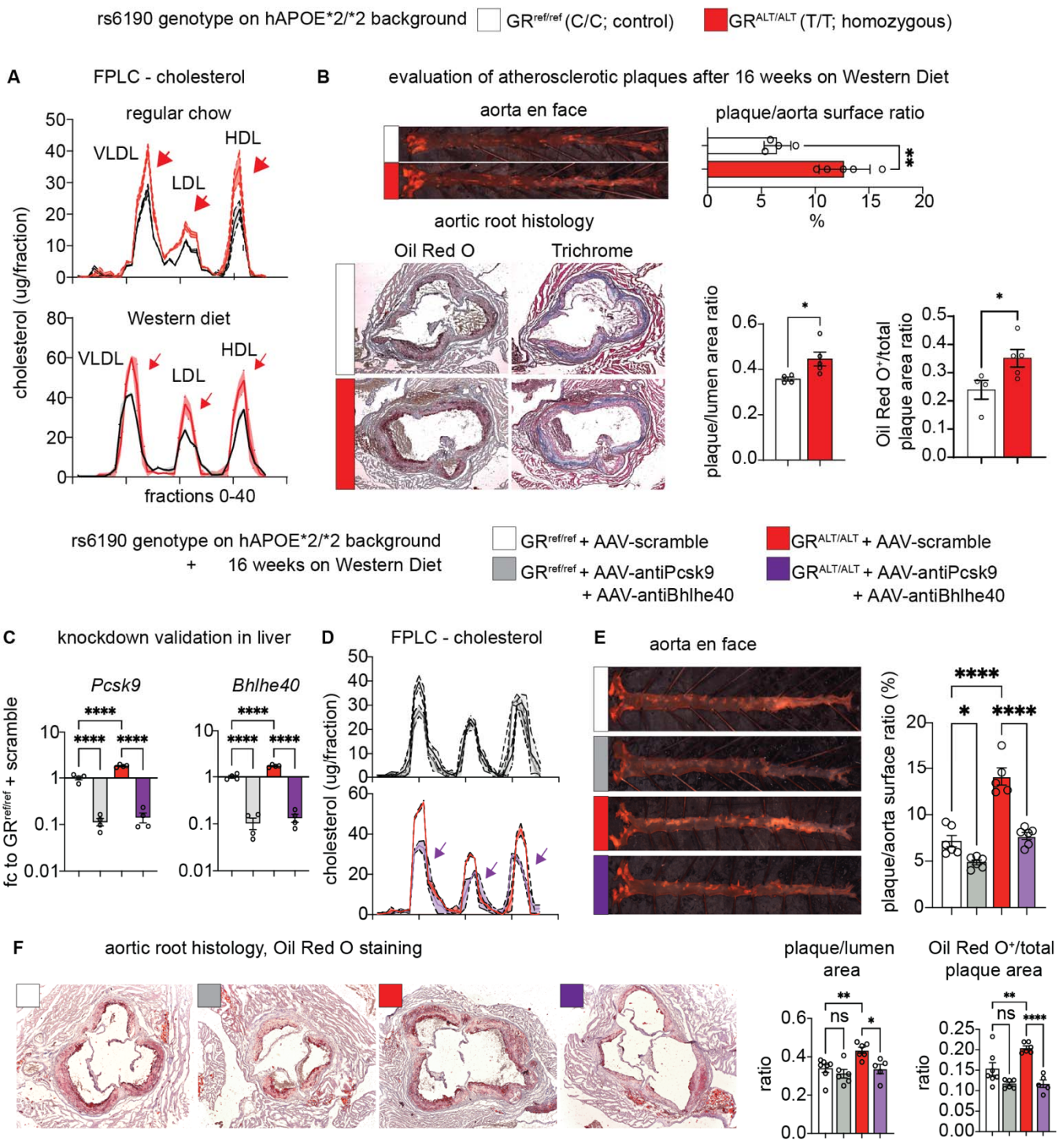

Figure 4. The SNP promotes atherosclerosis in vivo. (A) FPLC curves show the additive effect of SNP genotype on the hAPOE*2/*2-driven hypercholesterolemia across lipoprotein fractions in both normal and Western diets (arrows). **(B)** Compared to $GR^{ref/ref}$ mice, $GR^{ALT/ALT}$ mice on the *hAPOE*2/*2* background showed higher incidence (as quantitated from en face analyses) and severity (as quantitated through Oil Red O staining in aortic root sections) of atherosclerotic plaques. **(C)** qPCR validation of target knockdown in liver. **(D-F)** AAV-mediated knockdown of *Pcsk9* and *Bhlhe40* in adult mice blunted the SNP effect on VLDL-, LDL- and HDL-cholesterol (FPLC), plaque incidence in en face aorta assays, and histological severity of aortic root plaques. N=4-7♀/group, 6mo; B: Welch's t-test; E-F: 2w ANOVA + Sidak; *, P<0.05; **, P<0.01; ***, P<0.001; ****, P<0.0001.

Supplementary Figure 1

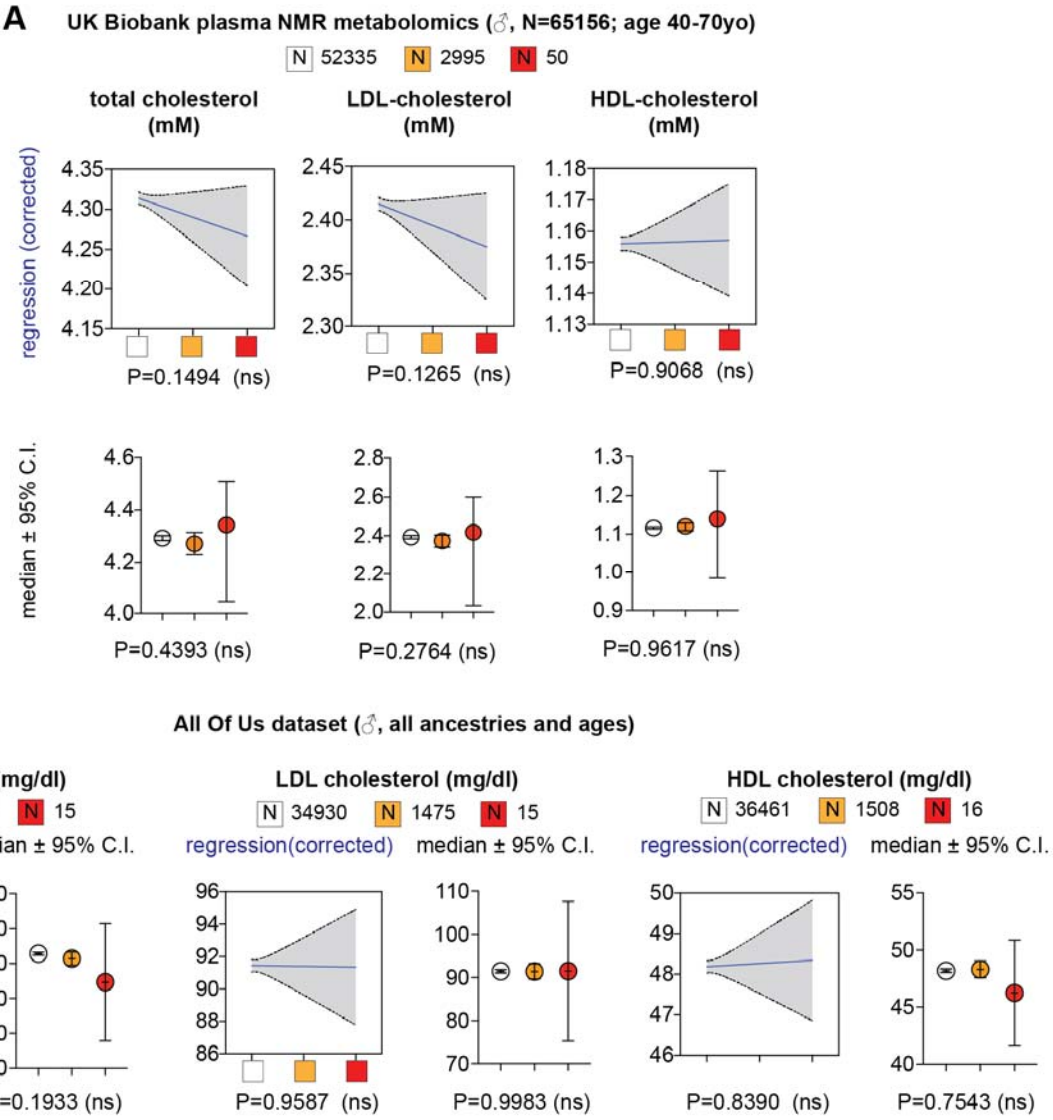

Supplementary Figure 1. Related to Figure 1. Additional data from UK Biobank and All Of Us datasets. Zygosity-dependent correlations of rs6190 with total, LDL and HDL cholesterol were not significant in men from either UK Biobank (A) or All of Us (B) datasets. Linear regressions were corrected for age, diabetes, triacylglycerols; median intervals were compared through Kruskal-Wallis test.

Supplementary Figure 2

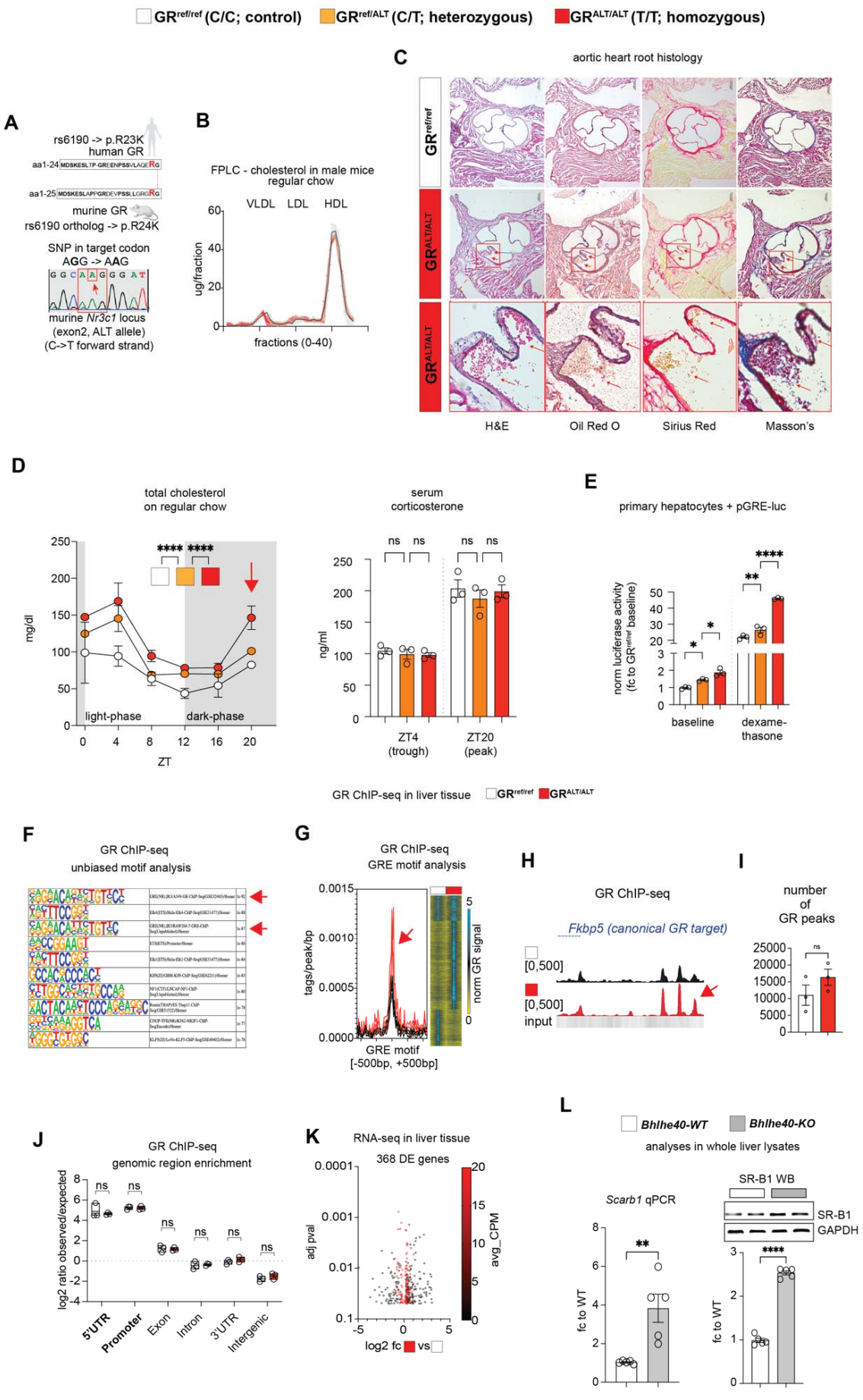

Supplementary Figure 2. Related to Figure 2. Additional analyses related to mutant GR effects in murine liver. (A) Diagram highlighting the human-mouse GR sequence orthology and the SNP genocopy introduced through CRISPR-Cas9. **(B)** Differently than in female mice, male mice blunted the SNP effect on cholesterol elevation according to SNP zygosity, according to FPLC cholesterol levels across lipoprotein fractions. **(C)** In 3 out of 5 female mice analyzed from the parental WT genetic background after Western diet exposure, emerging immature plaques were noted in the aortic roots (arrows; insets: high magnification). **(D)** The SNP effect on cholesterol in female mice followed circadian fluctuations and peaked in the active phase (dark phase; arrow), in phase with the endogenous corticosterone elevation in mice. However, no SNP-dependent effects were noted in either peak or trough corticosterone values (right histogram). **(E)** The SNP increased basal and steroid-driven GR activity on a GRE luciferase reporter transfected in primary hepatocytes. **(G)** Unbiased motif analysis validates ChIP-seq datasets through enrichment for GRE motif (arrows). **(H)** Mutant GR showed increased GR occupancy genome-wide on GRE motifs (arrow). **(I)** Representative peak traces for a canonical marker of GR epigenetic activity, the *Fkbp5* distal promoter (arrow). **(J)** Mutant GR had a higher number of peaks than the control GR, although the relative genomic distribution did not change. **(K)** Volcano plot of SNP-dependent differentially expressed genes in liver per RNA-seq datasets. **(L)** Compared to *Bhlhe40-WT* littermates, *Bhlhe40-KO* livers showed upregulation of SR-B1 levels at mRNA (*Scarb1*, gene name for SR-B1), supporting the notion of Bhlhe40 as transcriptional repressor of SR-B1 in liver. N=3-5/group, ♂ in B, ♀ in C-L, 6mo; D, E, J: 2w ANOVA + Sidak; I, L: Welch's t-test; *, P<0.05; **, P<0.01; ***, P<0.001; ****, P<0.0001.

Supplementary Figure 3

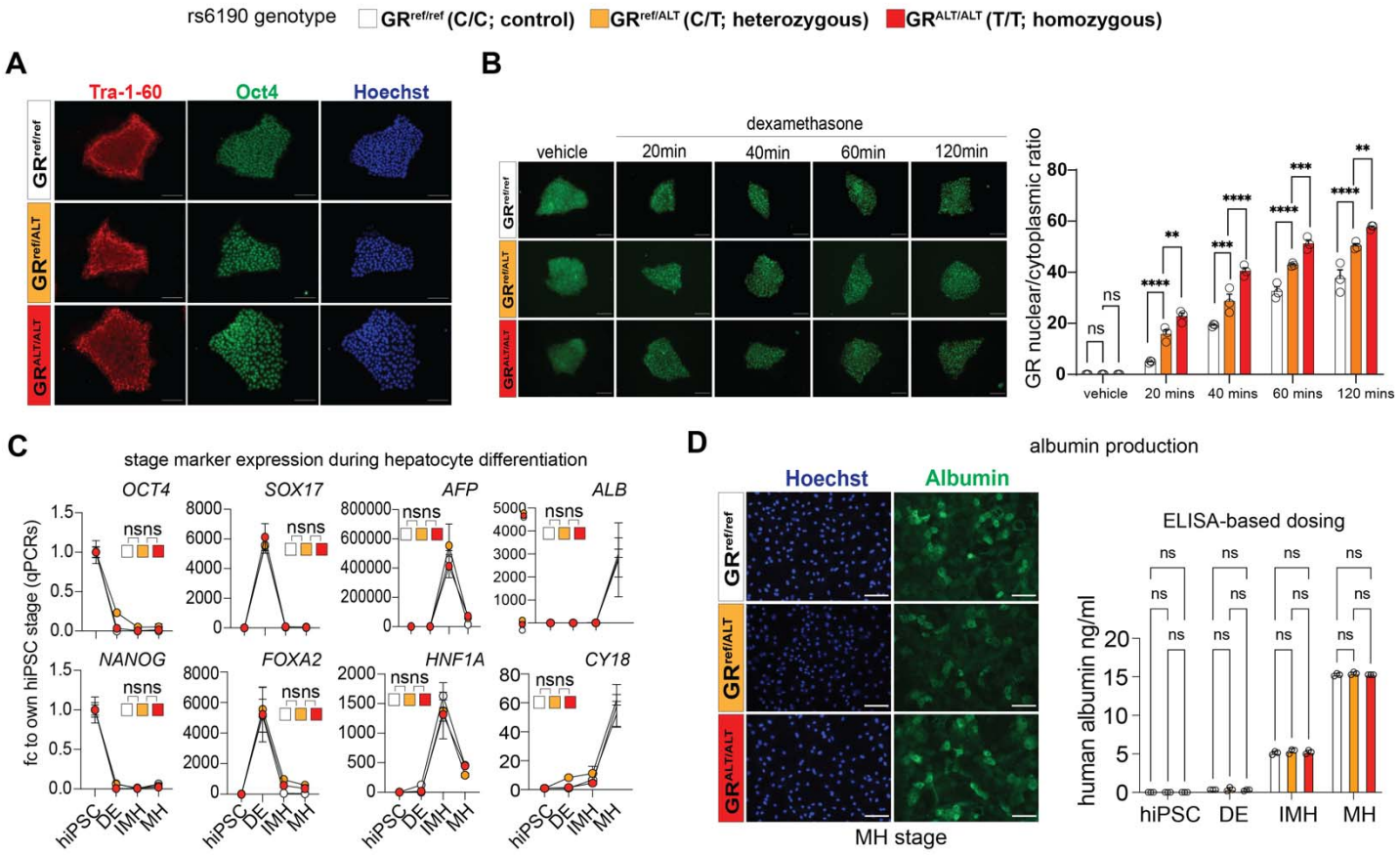

Supplementary Figure 3. Related to Figure 3. Additional analyses related to SNP-mutant hiPSCs. (A) Pluripotency marker validation of isogenic hiPSC lines with CRISPR-knock-in engineering of a SNP genocopy in the endogenous *NR3C1* gene locus. **(B)** The SNP promoted GR translocation at the undifferentiated hiPSC stage. **(C)** The SNP genotype did not impact the overall progression of differentiating hiPSCs across the stages of hepatocyte differentiation: hiPSC, pluripotent; DE, definitive endoderm; IMH, immature hepatocytes; MH, mature hepatocytes. (D) Albumin production (staining) and secretion (ELISA) confirmed hepatocyte maturation comparable across SNP genotypes. Each dot represents an independent differentiation replicate; N=3/group. 2w ANOVA + Sidak; *, P<0.05; **, P<0.01; ***, P<0.001; ****, P<0.0001.

Supplementary Figure 4

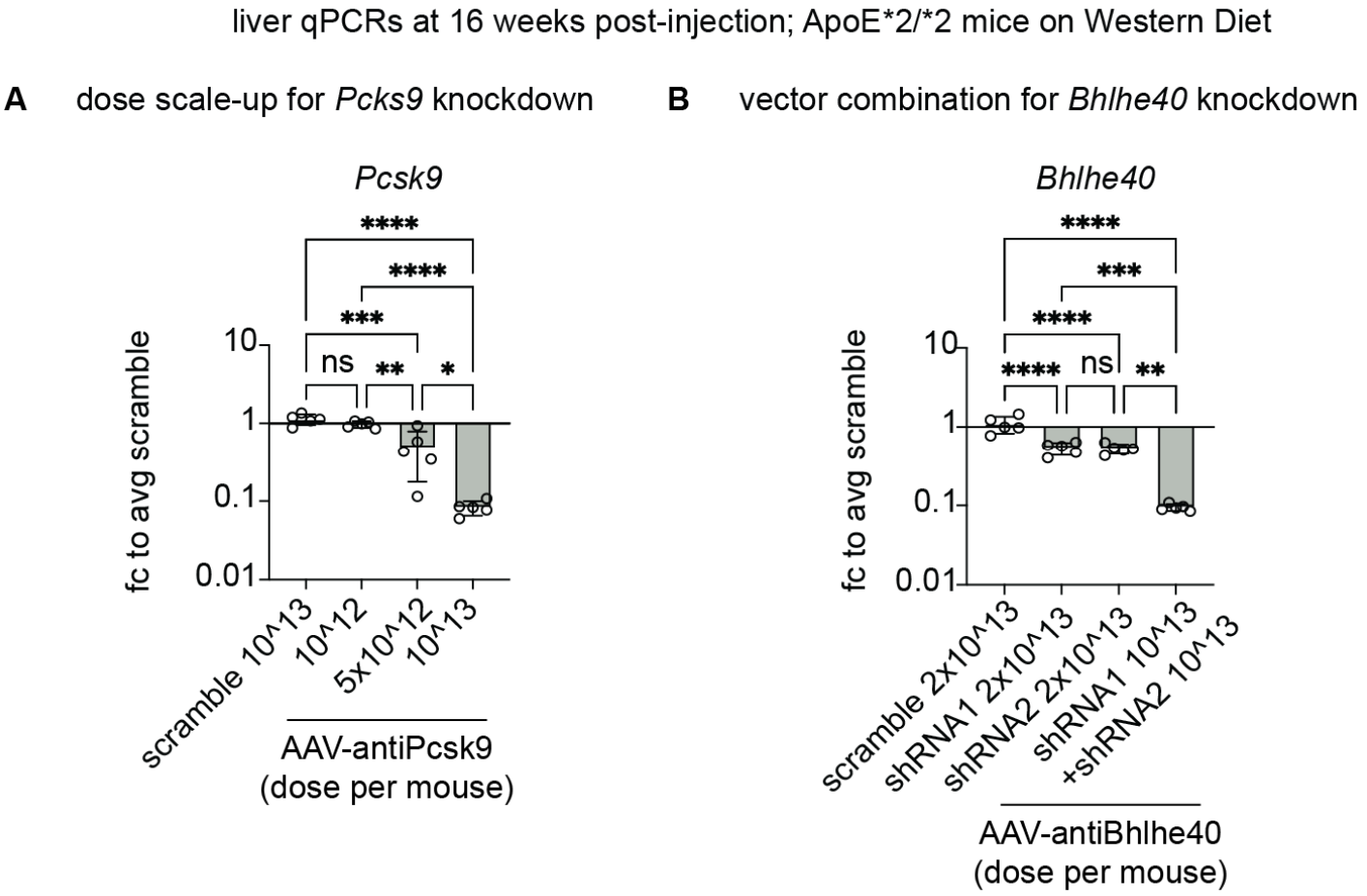

Supplementary Figure 4 – Preliminary validations of dosage and combinations for AAV8-mediated knockdowns in vivo. (A) 10^13vg/mouse maximized *Pcsk9* knockdown in liver with AAV8-antiPcsk9 compared to scramble. **(B)** Combination of both AAV8-antiBhlhe40 shRNA vectors was synergistic in maximizing *Bhlhe40* knockdown in liver compared to scramble. N=5♀/group, 6mo; 1w ANOVA + Sidak; *, P<0.05; **, P<0.01; ***, P<0.001; ****, P<0.0001.

METHODS

Animals and diet

Mice used in this study were maintained in a pathogen-free facility in accordance with the American Veterinary Medical Association (AVMA) and under protocol fully approved by the Institutional Animal Care and Use Committee (IACUC) at Cincinnati Children's Hospital Medical Center (#2023-0002). Euthanasia of the mice was carried out in accordance with ethical guidelines. Carbon dioxide inhalation was utilized as the initial method for euthanasia, followed by cervical dislocation and removal of the liver tissue.

All animals were maintained in a temperature-controlled environment with a 12h/12h light/dark cycle. For the fasting group, mice were subjected to an 18-hour starvation period. Mutant GR mice were generated using CRISPR/Cas9 genome editing by genocopying the rs6190 SNP in the endogenous *Nr3c1* locus on the C57BL/6J background. This genetic modification was performed by the Transgenic Animal and Genome Editing Core Facility at CCHMC. To ensure genetic background homogeneity and control for potential confounding variables, the colonies were maintained through heterozygous matings. This approach allowed us to compare three distinct groups of mice as littermates: $GR^{ref/ref}$ (control WT), $GR^{ref/ALT}$ (heterozygous SNP carriers), and $GR^{ALT/ALT}$ (homozygous SNP carriers). All animals used in this study were approximately 3-4 months of age at the time of experimentation. As the primary atherogenic model, *hAPOE*2/*2* homozygous mice were originally obtained from the Maeda Laboratory at the University of North Carolina (44) and maintained as breeding colony from Dr. David Hui's lab at the University of Cincinnati. These mice were crossed with the R24K mutant mice. To induce hypercholesterolemia and atherosclerosis, R24K mice crossed on *hAPOE*2/*2* background were subjected to cholate-free western diet, which contained 21% fat and 0.2% cholesterol for 16 weeks.

For systemic AAV experiments, wild-type and homozygous SNP-mutant littermate mice on *hAPOE*2/*2* background were injected retro-orbitally with either $3x10^{13}$ vg/mouse of AAV8-scramble shRNA or $1x10^{13}$ vg/mouse for each of the knockdown combination vectors, i.e. one AAV8-anti*Pcsk9* (46) and two AAV8-*Bhlhe40*shRNA vectors (Vector Builder vectors # VB010000-0023jze, VB230421-1310pka, VB230421-1312ydp; Addgene #163025; scramble shRNA sequence: CCTAAGGTTAAGTCGCCCTCG; anti-*Bhlhe40* shRNA sequences: GCGAGGTTACAGTGTTTATAT, GTAGTGGTTTGGGCAAATTTC) while under inhaled isoflurane anesthesia. All AAV8 injections were diluted in sterile PBS. To prepare and isolate AAV virions, we followed the procedures we previously reported (54, 55).

RNA extraction and RT-qPCR

Total RNA was extracted from cryo-pulverized liver tissues and hiPSC-derived hepatocyte-like cells using Trizol (Cat #15596026, Thermo Fisher Scientific) and 1 ug RNA was reverse-transcribed using SuperScript™ IV VILO™ Master Mix (Cat #11756050, Thermo Fisher Scientific). RT-qPCRs were conducted in three replicates using 1X SYBR Green Fast qPCR machine (Bio-Rad, Hercules, CA; thermal profile: 95C, 15 sec; 60C, 30sec; 40x; melting curve). The 2-ΔΔCT method was used to calculate relative gene expression. GAPDH was used as the internal control. Primers were selected among validated primer sets from MGH PrimerBank:

Gene Name	Forward sequence	Reverse Sequence
Mouse *Pcsk9*	GAGACCCAGAGGCTACAGATT	AATGTACTCCACATGGGGCAA
Mouse *Bhlhe40*	ACGGAGACCTGTCAGGGATG	GGCAGTTTGTAAGTTTCCTTGC
Mouse *Scarb1*	TTTGGAGTGGTAGTAAAAAGGGC	TGACATCAGGGACTCAGAGTAG
Mouse *Ldlr*	TGACTCAGACGAACAAGGCTG	ATCTAGGCAATCTCGGTCTCC
Mouse *Gapdh*	GTATGACTCCACTCACGGCAAA	GGTCTCGCTCCTGGAAGATG
Human *OCT4*	AGCGAACCAGTATCGAGAAC	TTACAGAACCACACTCGGAC
Human *NANOG*	CTCCAACATCCTGAACCTCAGC	CGTCACACCATTGCTATTCTTCG
Human *SOX17*	TATTTTGTCTGCCACTTGAACAGT	TTGGGACACATTCAAAGCTAGTTA
Human *FOXA2*	GCATTCCCAATCTTGACACGGTGA	GCCCTTGCAGCCAGAATACACATT
Human *NESTIN*	CTGCTACCCTTGAGACACCTG	GGGCTCTGATCTCTGCATCTAC
Human *PAX6*	AACGATAACATACCAAGCGTGT	GGTCTGCCCGTTCAACATC
Human *TBX6*	GTGTCTTTCCATCGTGTCAAGC	TATGCGGGGTTGGTACTTGTG
Human *MIXL1*	GGCGTCAGAGTGGGAAATCC	GGCAGGCAGTTCACATCTACC
Human *ALB*	CCCCAAGTGTCAACTCCA	GTTCAGGACCACGGATAG
Human *AFP*	ACTGAATCCAGAACACTGCA	TGCAGTCAATGCATCTTTCA
Human *HNF1A*	ACATGGACATGGCCGACTAC	CGTTGAGGTTGGTGCCTTCT
Human *CY18*	GCTGGAAGATGGCGAGGACTTT	TGGTCTCAGACACCACTTTGCC
Human *PCSK9*	GACACCAGCATACAGAGTGACC	GTGCCATGACTGTCACACTTGC
Human *BHLHE40*	TAAAGCGGAGCGAGGACAGCAA	GATGTTCGGGTAGGAGATCCTTC
Human *SCARB1*	GGTCCAGAACATCAGCAGGATC	GCCACATTTGCCCAGAAGTTCC
Human *LDLR*	GAATCTACTGGTCTGACCTGTCC	GGTCCAGTAGATGTTGCTGTGG
Human *GAPDH*	GTCTCCTCTGACTTCAACAGCG	ACCACCCTGTTGCTGTAGCCAA

Western blotting

Protein analyses in liver were performed on ~ 25 ug total lysates. Cyro-pulverized liver tissue was incubated in RIPA buffer (Cat #89900Thermo Fisher Scientific) supplemented with 1x protease/phosphatase inhibitor (Cat #78440, Thermo Fisher Scientific) for 30 mins and sonicated for 10 secs twice. The samples were then centri-

fuged at 12,000 rpm for 10 mins at 4^{o}C. Supernatant containing the protein is transferred into a new tube and used as a total lysate. For total cell lysates from culture cells, cells were harvested and resuspended in RIPA buffer containing 1x protease and phosphatase inhibitors. Lysates were incubated for 30 mins and centrifuged at 12,000 rpm for 10 mins at 4^{o}C. The supernatant was used as a total cell lysate. The protein concentrations of the supernatants were determined using the Pierce BCA Protein Assay kit (Cat #23225, Thermo Fisher Scientific). Equal amounts of protein were separated using SDS-PAGE and transferred to a PVDF membrane (Cat #1620177, BioRad). Membranes were blocked in 5% milk in TBST for 1 hour at room temperature and then incubated overnight at 4^{o}C with primary antibodies: PCSK9 (Cat #A7860, 1:1000, ABclonal), BHLHE40 (Cat #A6534, 1:1000, ABclonal), SR-B1 (Cat #A0827, 1:1000, ABclonal), LDLR (Cat #A14996, 1:1000, ABclonal), followed by incubation with anti-rabbit IgG, HRP-conjugated secondary antibody (Cat #7074, 1:5000, Cell Signaling) for 1 hour at room temperature. Immunoreactive bands were visualized by chemiluminescence using Pierce Enhanced Chemiluminescent western blotting substrate (Cat #32106, Thermo Fisher Scientific)

RNA sequencing sample preparation and analysis

RNA-seq was conducted on RNA extracted from the liver tissue of wild-type versus R24K homozygous mice. Each liver was immediately snap frozen in 1 ml TRIsure (Bioline, BIO-38033) using liquid Nitrogen. RNAs from each heart were extracted individually and re-purified using the RNeasy Mini Kit (Cat #74104, Qiagen). RNA-seq was performed at the DNA core (CCHMC). 150 ng – 300 ng of total RNA determined by Qubit (Invitrogen) high-sensitivity spectrofluorometric measurement was poly-A selected and reverse transcribed using Illumina's TruSeq stranded mRNA library preparation kit (Cat #20020595, Illumina, San Diego, CA). Each sample was fitted with one of 96 adapters containing a different 8 base molecular barcode for high level multiplexing. After 15 cycles of PCR amplification, completed libraries were sequenced on an Illumina NovaSeqTM 6000, generating 20 million or more high quality 100 base long paired end reads per sample. A quality control check on the fastq files was performed using FastQC. Upon passing basic quality metrics, the reads were trimmed to remove adapters and low-quality reads using default parameters in Trimmomatic [Version 0.33]. The trimmed reads were then mapped to mm10 reference genome using default parameters with strandness (R for single-end and RF for paired-end) option in Hisat2 [Version 2.0.5]. Next, the transcript/gene abundance was determined using kallisto [Version 0.43.1]. We first created a transcriptome index in kallisto using Ensembl cDNA sequences for the reference genome. This index was then used to quantify transcript abundance in raw counts and counts per million (CPM). Differential expression (DE genes, FDR<0.05) was quantitated through DESeq2. PCA was conducted using ClustVis. Gene ontology pathway enrichment was conducted using the Gene Ontology analysis tool.

Chromatin immunoprecipitation sequencing

Whole livers were cryopowdered using a liquid nitrogen-cooled RETSCH CryoMill. The cryopowdered tissue was then fixed in 10 ml of 1% paraformaldehyde (PFA) for 30 mins at room temperature with gently nutation. Fixation was quenched 1ml of 1.375 M glycine (Cat # BP381-5, Thermo Fisher Scientific) with gentle nutation for 5 min at room temperature. After centrifugation at 3000g for 5 mins at 4^{o}C, the pellet was resuspended in

cell lysis buffer as per reported conditions, supplementing the cell lysis buffer with cytochalasin B (3 ug/ml) and rotating for 10 min at 4^{o}C. Nuclei were pelleted at 300g for 10 min at 4^{o}C and subsequently processed following the reported protocol with the adjustment of adding cytochalasin B (3ug/ml) into all solutions for chromatin preparation and sonication, antibody incubation, and wash steps. Chromatin was then sonicated for 15 cycles (30s, high power, 30s pause, and 500 µl volume) in a water bath sonicator set at 4^{o}C (Bioruptor 300. Diagenode, Denville, NJ). After centrifuging at 10,000g for 10 min at 4^{o}C, sheared chromatin was checked on agarose gel for a shear band comprised between 150 and 600 bp. Two micrograms of chromatin were kept for pooled input controls, whereas 50 ug of chromatin was used for each pull-down reaction in a final volume of 2ml rotating at 4^{o}C overnight. Rabbit polyclonal anti-GR (Cat # A2164, 1:100, ABclonal) was used as a primary antibody. Chromatin complexes were precipitated with 100 µl of Sheep Dynabead M-280 (Cat #11204, Thermo Fisher). After washing and elution, samples were treated with proteinase K (Cat #19131, Qiagen) at 55^{o}C, cross-linking was reversed through overnight incubation at 65^{o}C. DNA was purified using a MinElute purification kit (Cat #28004, Qiagen) and quantified using Qubit reader and reagents. Library preparation and sequencing were conducted at the NU Genomics Core, using TrueSeq ChIP-seq library prep (with size exclusion) on 10 ng of chromatin per ChIP sample or pooled inputs and HiSeq 50-bp single-read sequencing (60 million read coverage per sample). Peak analysis was conducted using HOMER software (v4.10) after aligning fastq files to the mm10 mouse genome using bowtie2. PCA was conducted using ClustVis. Heatmaps of peak density were imaged with TreeView3. Peak tracks were imaged through WashU epigenome browser. Gene ontology pathway enrichment was conducted using the gen ontology analysis tool.

Plasma measurements of total cholesterol and total triglycerides

Blood samples were procured from ~3-month-old mice and collected in EDTA-treated tubes using cardiac puncture method following an overnight fasting. The blood samples were maintained on ice and subjected to centrifugation at 2500 x g for 10 mins to isolate plasma. Following the centrifugation step, the obtained plasma was immediately transferred into a clean microcentrifuge tube for plasma lipid measurements. The plasma levels of total cholesterol (TC) and total triglycerides (TG) were measured using Infinity^{TM} Cholesterol kit (Cat #TR13421, Thermo Fisher Scientific) and Infinity^{TM} Triglyceride kit (Cat # TR22421, Thermo Fisher Scientific).

Lipoprotein analysis

For lipoprotein separation through FPLC, fresh plasma samples were pooled, totaling 250 µl, obtained from at least 5 mice per group. Each group's pooled plasma underwent FPLC gel filtration, utilizing a tandem arrangement of 2 Superose 6 columns (GE Healthcare). The elution process entailed the collection of fractions in 0.5 ml increments, maintaining a steady flow rate of 0.5 ml/min. This procedure yields a total of fifty-one distinct fractions, each of which is subjected to quantification of total triglyceride and cholesterol levels using the Infinity Triglyceride and Cholesterol kits.

Atherosclerotic lesion analysis

Mice under anesthesia were subjected to a perfusion procedure using a 10% formalin solution in buffered saline for 5 mins. Following this perfusion, the hearts were carefully dissected to harvest aortic roots. These harvested tissues were subsequently preserved in 10% buffered formalin solution. To assess the distribution of atherosclerosis, en face whole aorta lesion staining was performed with Oil Red O for 30 mins, followed by two 1x PBS washes. Furthermore, the aortic root of the heart was embedded in OCT compound for the preparation of frozen sections. Cross cryosections of the aortic roots, measuring 7µm in thickness and encompassing the aortic valve region, were stained with H&E, Oil Red O and Trichrome staining according to our established protocols. Images were obtained using a ZEISS Axio Imager.A2 microscope and histological analyses performed using the ImageJ software (NIH).

Human iPSC cell line and maintenance

Human iPSC line 72_3 with CRISPR knock-in for R23K in the *Nr3c1* gene locus to generate heterozygous and homozygous for GR SNP were obtained from CCHM Pluripotent Stem Cell Facility (PSCF). The hiPSCs were maintained in feeder-free conditions using mTeSR1 medium (Cat #85850, StemCell Technologies) in a humidified incubator at 37^{o}C, 5% CO_2. Human iPSCs were plated on six-well plates pre-coated with Cultrex obtained from the CCHMC PSCF. The isogenic cell lines were tested and confirmed mycoplasma-free during maintenance and before differentiation process. For maintenance of hiPSC, the cells at 70% confluency were passaged using Gentle Cell Dissociation Reagent (GCDR) (Cat #100-0485, StemCell Technologies) into medium clumps. The colonies were resuspended in mTeSR^{TM}1 medium with 10 µM Y-27632 (PSCF, CCHMC) and passaged at split ratios ranging from 1:6 to 1:9 as appropriate.

Human iPSC-derived hepatocyte-like cells (HLCs) differentiation in vitro

When human iPSCs reached a confluency of approximately 95% they were passaged with Accutase^{TM} Cell Dissociation Reagent (Cat #07920, StemCell Technologies) and resuspended as single cells in mTesR^{TM}1 medium with 10 µM Y-27632 (Tocris Bioscience). The cells were seeded in six well plates pre-coated with Cultrex diluted in ice-cold DMEM/F12 (Thermo Fisher Scientific). After 24 hours, wash the cells with room temperature DMEM/F12 and switch to RPMI 1640 (Cat #11875093, Thermo Fisher Scientific) with B27 supplement Minus Insulin (Cat #A1895601, Thermo Fisher Scientific), along with 100 ng/ml Activin A (Cat #120-14P, Peprotech) and 3 µM CHIR99021 (Cat #4423, Tocris Bioscience). Following 24-h treatment, CHIR99021 was withdrawn, and the cells were treated with RPMI 1690/B27 Minus Insulin basal medium with 100 ng/ml Activin A for another 48 hours and renewed every day to generate definitive endoderm cells (DE). The differentiated endoderm cells were further treated with RPMI 1640/B27 Minus Insulin along with 10 ng/ml basic fibroblast growth factor (FGF) (Cat 3100-18B, Peprotech) and 20 ng/ml Bone morphogenic factor 4 (BMP4) (Cat #120-05ET, Peprotech). The media was replaced every day for the next 5 days to generate hepatic progenitor (HP) cells. Next, the hepatic progenitors were further differentiated into immature hepatocytes (IMH) by replacing the media with RPMI/B27 Minus Insulin, 20 ng/ml hepatocyte growth factor (HGF) (Cat #100-39, Peprotech), and 0.5% DMSO. The media was replaced every day for the next 5 days. To promote maturation of immature hepatocytes, the media was replaced with HCM^{TM} Hepatocyte Culture Medium Bulletkit^{TM} (Cat # CC-3198,

Lonza) except HEGF, 10 ng/ml HGF, 20 ng/ml Oncostatin M (Cat #300-10T, Peprotech), 100 nM Dexamethasone (Cat # D2915, Sigma), and 0.5% DMSO for another 5 days with everyday media change.

For the GR translocation assay and analysis, hiPSCs were exposed to either a vehicle control or 1 µM Dexamethasone for various time intervals (20 mins, 40 mins, 60 mins, and 120 mins). Subsequently, an immunofluorescence assay was performed. To evaluate GR translocation in hiPSC-derived mature HLCs, the maturation medium containing 100 nM Dexamethasone was removed, and the cells were cultured in hepatocyte maintenance (HCM) medium without dexamethasone for 24 hours. The following day, mature HLCs were treated with either a vehicle control or 1 µM Dexamethasone for the aforementioned time intervals. Immunofluorescent staining was performed using GR (Cat #sc-393232, 1:200, Santa Cruz) and Alexa Fluor® 488 AffiniPure Donkey Anti-Mouse IgG (H+L) (Cat #102650-156, 1:300, VWR). The analysis of GR translocation was carried out using ImageJ software on 5-6 images per sample acquired from a Nikon Eclipse Ti-U microscope.

Human Albumin ELISA

Cell supernatant containing the cell culture media from mature hiPSC-hepatocytes was collected and centrifuged at 2000 x g for 10 mins to remove debris. Centrifuged samples were diluted 1:5 in Sample Diluent NS provided in the kit (Cat # ab179887, Abcam) and assayed according to the manufacturer's instructions.

Isolation of Primary mouse hepatocytes

Primary hepatocytes were isolated from $GR^{ref/ref}$ (control), $GR^{ref/ALT}$ (het), and $GR^{ALT/ALT}$ (homo) mice with collagenase perfusion method. The mice were anesthetized, and the inferior vena cava (IVC) was cannulated with a 24-gauge needle. HBSS – (Cat #14175095, Thermo Fisher Scientific) containing 0.5 mM EDTA (Cat # AM9260G, Thermo Fisher Scientific) was perfused to chelate calcium. Next, HBSS + (Cat #14025092, Thermo Fisher Scientific) containing 0.3 mg/ml collagenase X (Cat #035-17861, FUJUFILM Wako Chemicals) was perfused to dissociate extracellular matrix of the liver. After the liver dissection, cells were filtered with 100 µm mesh cell strainer (Cat #08-771-19, Fisher Scientific), and the hepatocytes were purified by 40% Percoll (Cat # P1644, Sigma) gradient centrifugation method. Hepatocytes were suspended in William's E medium (Cat #12551032, Thermo Fisher Scientific) supplemented with 10% FBS (Cat # S11150, R&D systems) and 1x Anti-Anti (Cat #15240062, Thermo Fisher Scientific) for overnight and then replaced the next day with fresh medium.

Immunostaining and image analysis

Cells plated on cultrex-coated dishes containing sterile cover glasses were washed gently with 1x DPBS and fixed with Fixation solution (2% formaldehyde in 1x PBS) for 15 mins at room temperature. The cells were washed 3 times with 1x DPBS and treated with permeabilization reagent (1% triton X-100 in 1x DPBS) at 37^{o}C for 30 mins and then at room temperature for 10 mins. Next, the cells were blocked with blocking buffer (10% normal donkey serum in 1x DPBS) for 1 hour at room temperature and stained with primary antibodies: Nanog (Cat #D73G4, 1:200, Cell Signaling), OCT4 (Cat #A7920, 1:200, ABclonal), and Albumin (Cat #A1363, 1:200, ABclonal) diluted in 10% Donkey serum in 1x DPBS overnight. Next day, the cells were washed twice with 1x

DPBS and stained with secondary antibodies: Alexa Fluor® 594 AffiniPure Donkey Anti-Rabbit IgG (H+L) (Cat #102649-732, 1:300, VWR), and Alexa Fluor® 488 AffiniPure Donkey Anti-Rabbit IgG (H+L) (Cat #102649-726, 1:300, VWR) diluted in 10% Donkey serum in 1x DPBS for 1 hour at room temperature. Cells were washed three times in 1x DPBS. The coverslips were mounted on slides and imaged with Nikon Eclipse Ti – U microscope.

Fluorometric HDL and LDL uptake assay and quantitation

Plate 3-4x10^4 cells/ well in a 96-well white clear-bottom cell culture plates and culture in media overnight at 37^{o}C incubator. Next day, wash the cells with Assay buffer provided in this appropriate kit. For fluorometric HDL (Cat #ab204717, Abcam) and LDL (Cat #770230-9, Kalen Biomedical) staining and quantitation, follow the instructions according to the manufacturer. Protect from light and measure the fluorescence in a microplate reader.

UK Biobank and All of Us analyses

Our analyses were conducted under the UKB application number 65846 and All of Us workspace number aourw-0fb52975. We constructed a rs6190 genotype-stratified cohort, excluding participants if they withdrew consent. All available values for the tested parameters were collected per genotype group. For UK Biobank, UDI and related parameters: Age: 21001-0.0; BMI: 21001-0.0; Glycemia (mM): 30740-0.0; Triglycerides (mM): 30870-0.0; Total Cholesterol: 23400; ICD10 causes of death, primary 40001, secondary 40002. For initial discovery using the NMR metabolomics datasets, quantitative linear regression and conditional analyses were performed using an additive genetic model adjusting for 10 PCs, sex; and age. In conditional analyses, the 12 established SNP dosage effects were also included as additional covariates. Regression analyses were performed using second generation of PLINK (56). Before analyses, a series of standard QC measures were applied including sample call rates, sample relatedness, and sex inconsistency as well as marker quality (i.e., marker call rate, minor allele frequency (MAF), and Hardy-Weinberg equilibrium (HWE). Analyses were limited to participants with call rates >□98%, SNPs with call rates >□99%, and SNPs with MAF >□1% and HWE p□>□0.0001. For independent association confirmation studies, multiple linear regression analysis was carried out using R 4.3.2 (R Core Team, 2023) to explore the association of total cholesterol, clinical LDL, and HDL cholesterol versus separate sex (males/females) and correcting for BMI, glycemia, and triglycerides.

Statistics

Unless differently noted, statistical analyses were performed using Prism software v8.4.1 (GraphPad, La Jolla, CA). The Pearson-D'Agostino normality test was used to assess data distribution normality. When comparing the two groups, a two-tailed Student's t-test with Welch's correction (unequal variances) was used. When comparing three groups of data from one variable, one-way ANOVA with Sidak multi-comparison was used. When comparing data groups for more than one related variable, two-way ANOVA was used. For ANOVA and t-test analyses, a P value less than 0.05 was considered significant. When the number of data points was less than 10, data were presented as single values (dot plots, histograms). Tukey distribution bars were used to empha-

size data range distribution in analyses pooling larger data points sets per group (typically > 10 data points). Analyses pooling data points over time were presented as line plots connecting medians of box plots showing distribution of all data per time points. Randomization and blinding practices are followed for all experiments. All the data from all animal cohorts and cell clone replicates is reported, whether outlier or not.

Study approval

Mice were housed in a pathogen-free facility in accordance with the American Veterinary Medical Association (AVMA) and under protocols fully approved by the Institutional Animal Care and Use Committee (IACUC) at Cincinnati Children's Hospital Medical Center (#2022-0020, #2023-0002). UKB and All of Us analyses were conducted under the UKB application number 65846 and All of Us workspace number aou-rw-0fb52975.

Data availability

RNA-seq and ChIP-seq datasets reported here are available on GEO as GSE280494 and GSE280572. Individual data for all charts presented here is available in the Supporting Data Values file.

Author contributions –HBD, AH, GN, ADP, KMF, HL, OA, BNK: Data curation, Formal analysis, Investigation; AJ, DYH: Resources; MQ: Conceptualization, Formal analysis, Funding acquisition, Supervision.

Acknowledgements - Next-gen sequencing was performed thanks to the Cincinnati Children's DNA Sequencing and Genotyping Facility (RRID: SCR_022630), with critical assistance by David Fletcher, Keely Icardi, Julia Flynn, and Taliesin Lenhart. hiPSC generation, engineering and initial quality control/selection were performed thanks to the Cincinnati Children's Pluripotent Stem Cell Facility (RRID: SCR_022634), with critical assistance by Chris Mayhew and Yueh-Chiang Hu. pAAV Alb-AAT KRAB-SadCas9 U6-mPcsk9 was a gift from Tonia Rex (Addgene plasmid # 163025 ; http://n2t.net/addgene:163025 ; RRID:Addgene_163025).

Grant support – This work was supported by R56HL158531-01, R01HL166356-01, R03DK130908-01A1, R01AG078174-01 (NIH) and RIP, GAP, CCRF Endowed Scholarship, HI Translational Funds (CCHMC) grants to MQ; NIH grant RO1HL156954 to DYH.

References

1. Zamora A, Ramos R, Comas-Cufi M, Garcia-Gil M, Marti-Lluch R, Plana N, et al. Women with familial hypercholesterolemia phenotype are undertreated and poorly controlled compared to men. *Sci Rep.* 2023;13(1):1492.
2. Iyen B, Qureshi N, Weng S, Roderick P, Kai J, Capps N, et al. Sex differences in cardiovascular morbidity associated with familial hypercholesterolaemia: A retrospective cohort study of the UK Simon Broome register linked to national hospital records. *Atherosclerosis.* 2020;315:131-7.
3. de Guia RM, Rose AJ, and Herzig S. Glucocorticoid hormones and energy homeostasis. *Horm Mol Biol Clin Investig.* 2014;19(2):117-28.
4. Schaaf MJ, and Cidlowski JA. Molecular mechanisms of glucocorticoid action and resistance. *J Steroid Biochem Mol Biol.* 2002;83(1-5):37-48.
5. Lim HW, Uhlenhaut NH, Rauch A, Weiner J, Hubner S, Hubner N, et al. Genomic redistribution of GR monomers and dimers mediates transcriptional response to exogenous glucocorticoid in vivo. *Genome Res.* 2015;25(6):836-44.
6. Oakley RH, and Cidlowski JA. The biology of the glucocorticoid receptor: new signaling mechanisms in health and disease. *J Allergy Clin Immunol.* 2013;132(5):1033-44.
7. Watts LM, Manchem VP, Leedom TA, Rivard AL, McKay RA, Bao D, et al. Reduction of hepatic and adipose tissue glucocorticoid receptor expression with antisense oligonucleotides improves hyperglycemia and hyperlipidemia in diabetic rodents without causing systemic glucocorticoid antagonism. *Diabetes.* 2005;54(6):1846-53.
8. Petrichenko IE, Daret D, Kolpakova GV, Shakhov YA, and Larrue J. Glucocorticoids stimulate cholesteryl ester formation in human smooth muscle cells. *Arterioscler Thromb Vasc Biol.* 1997;17(6):1143-51.
9. Nashel DJ. Is atherosclerosis a complication of long-term corticosteroid treatment? *Am J Med.* 1986;80(5):925-9.
10. MacLeod C, Hadoke PWF, and Nixon M. Glucocorticoids: Fuelling the Fire of Atherosclerosis or Therapeutic Extinguishers? *Int J Mol Sci.* 2021;22(14).
11. Pujades-Rodriguez M, Morgan AW, Cubbon RM, and Wu J. Dose-dependent oral glucocorticoid cardiovascular risks in people with immune-mediated inflammatory diseases: A population-based cohort study. *PLoS Med.* 2020;17(12):e1003432.
12. Trusca VG, Fuior EV, Fenyo IM, Kardassis D, Simionescu M, and Gafencu AV. Differential action of glucocorticoids on apolipoprotein E gene expression in macrophages and hepatocytes. *PloS one.* 2017;12(3):e0174078.
13. Ayaori M, Sawada S, Yonemura A, Iwamoto N, Ogura M, Tanaka N, et al. Glucocorticoid receptor regulates ATP-binding cassette transporter-A1 expression and apolipoprotein-mediated cholesterol efflux from macrophages. *Arterioscler Thromb Vasc Biol.* 2006;26(1):163-8.
14. Cavenee WK, Johnston D, and Melnykovych G. Regulation of cholesterol biosynthesis in HeLa S3G cells by serum lipoproteins: dexamethasone-mediated interference with suppression of 3-hydroxy-3-methylglutaryl coenzyme A reductase. *Proc Natl Acad Sci U S A.* 1978;75(5):2103-7.
15. van Rossum EF, and Lamberts SW. Polymorphisms in the glucocorticoid receptor gene and their associations with metabolic parameters and body composition. *Recent Prog Horm Res.* 2004;59:333-57.
16. Yudt MR, and Cidlowski JA. The glucocorticoid receptor: coding a diversity of proteins and responses through a single gene. *Mol Endocrinol.* 2002;16(8):1719-26.
17. van Rossum EF, Koper JW, Huizenga NA, Uitterlinden AG, Janssen JA, Brinkmann AO, et al. A polymorphism in the glucocorticoid receptor gene, which decreases sensitivity to glucocorticoids in vivo, is associated with low insulin and cholesterol levels. *Diabetes.* 2002;51(10):3128-34.
18. Kino T. Single Nucleotide Variations of the Human GR Gene Manifested as Pathologic Mutations or Polymorphisms. *Endocrinology.* 2018;159(7):2506-19.
19. van Rossum EF, Feelders RA, van den Beld AW, Uitterlinden AG, Janssen JA, Ester W, et al. Association of the ER22/23EK polymorphism in the glucocorticoid receptor gene with survival and C-reactive protein levels in elderly men. *Am J Med.* 2004;117(3):158-62.
20. Hu W, Jiang C, Kim M, Yang W, Zhu K, Guan D, et al. Individual-specific functional epigenomics reveals genetic determinants of adverse metabolic effects of glucocorticoids. *Cell Metab.* 2021;33(8):1592-609 e7.
21. Koper JW, Stolk RP, de Lange P, Huizenga NA, Molijn GJ, Pols HA, et al. Lack of association between five polymorphisms in the human glucocorticoid receptor gene and glucocorticoid resistance. *Hum Genet.* 1997;99(5):663-8.

22. Saadatagah S, Jose M, Dikilitas O, Alhalabi L, Miller AA, Fan X, et al. Author Correction: Genetic basis of hypercholesterolemia in adults. *NPJ Genom Med.* 2021;6(1):56.
23. Trapani L, Segatto M, and Pallottini V. Regulation and deregulation of cholesterol homeostasis: The liver as a metabolic "power station". *World J Hepatol.* 2012;4(6):184-90.
24. Russo P, Tomino C, Santoro A, Prinzi G, Proietti S, Kisialiou A, et al. FKBP5 rs4713916: A Potential Genetic Predictor of Interindividual Different Response to Inhaled Corticosteroids in Patients with Chronic Obstructive Pulmonary Disease in a Real-Life Setting. *Int J Mol Sci.* 2019;20(8).
25. Zannas AS, Wiechmann T, Gassen NC, and Binder EB. Gene-Stress-Epigenetic Regulation of FKBP5: Clinical and Translational Implications. *Neuropsychopharmacology.* 2016;41(1):261-74.
26. Hollstein T, Vogt A, Grenkowitz T, Stojakovic T, März W, Laufs U, et al. Treatment with PCSK9 inhibitors reduces atherogenic VLDL remnants in a real-world study. *Vascul Pharmacol.* 2019;116:8-15.
27. Canuel M, Sun X, Asselin MC, Paramithiotis E, Prat A, and Seidah NG. Proprotein convertase subtilisin/kexin type 9 (PCSK9) can mediate degradation of the low density lipoprotein receptor-related protein 1 (LRP-1). *PloS one.* 2013;8(5):e64145.
28. Maxwell KN, Fisher EA, and Breslow JL. Overexpression of PCSK9 accelerates the degradation of the LDLR in a post-endoplasmic reticulum compartment. *Proc Natl Acad Sci U S A.* 2005;102(6):2069-74.
29. Lagace TA. PCSK9 and LDLR degradation: regulatory mechanisms in circulation and in cells. *Curr Opin Lipidol.* 2014;25(5):387-93.
30. Azmi S, Sun H, Ozog A, and Taneja R. mSharp-1/DEC2, a basic helix-loop-helix protein functions as a transcriptional repressor of E box activity and Stra13 expression. *J Biol Chem.* 2003;278(22):20098-109.
31. Honma S, Kawamoto T, Takagi Y, Fujimoto K, Sato F, Noshiro M, et al. Dec1 and Dec2 are regulators of the mammalian molecular clock. *Nature.* 2002;419(6909):841-4.
32. Rouillard AD, Gundersen GW, Fernandez NF, Wang Z, Monteiro CD, McDermott MG, et al. The harmonizome: a collection of processed datasets gathered to serve and mine knowledge about genes and proteins. *Database (Oxford).* 2016;2016.
33. Shen WJ, Azhar S, and Kraemer FB. SR-B1: A Unique Multifunctional Receptor for Cholesterol Influx and Efflux. *Annu Rev Physiol.* 2018;80:95-116.
34. Hamilton KA, Wang Y, Raefsky SM, Berkowitz S, Spangler R, Suire CN, et al. Mice lacking the transcriptional regulator Bhlhe40 have enhanced neuronal excitability and impaired synaptic plasticity in the hippocampus. *PloS one.* 2018;13(5):e0196223.
35. Peters DT, Henderson CA, Warren CR, Friesen M, Xia F, Becker CE, et al. Asialoglycoprotein receptor 1 is a specific cell-surface marker for isolating hepatocytes derived from human pluripotent stem cells. *Development.* 2016;143(9):1475-81.
36. Lu H, Lei X, Winkler R, John S, Kumar D, Li W, et al. Crosstalk of hepatocyte nuclear factor 4a and glucocorticoid receptor in the regulation of lipid metabolism in mice fed a high-fat-high-sugar diet. *Lipids Health Dis.* 2022;21(1):46.
37. Oyadomari S, Matsuno F, Chowdhury S, Kimura T, Iwase K, Araki E, et al. The gene for hepatocyte nuclear factor (HNF)-4alpha is activated by glucocorticoids and glucagon, and repressed by insulin in rat liver. *FEBS Lett.* 2000;478(1-2):141-6.
38. Engblom D, Kornfeld JW, Schwake L, Tronche F, Reimann A, Beug H, et al. Direct glucocorticoid receptor-Stat5 interaction in hepatocytes controls body size and maturation-related gene expression. *Genes Dev.* 2007;21(10):1157-62.
39. Bharathan SP, Manian KV, Aalam SM, Palani D, Deshpande PA, Pratheesh MD, et al. Systematic evaluation of markers used for the identification of human induced pluripotent stem cells. *Biol Open.* 2017;6(1):100-8.
40. Wang P, McKnight KD, Wong DJ, Rodriguez RT, Sugiyama T, Gu X, et al. A molecular signature for purified definitive endoderm guides differentiation and isolation of endoderm from mouse and human embryonic stem cells. *Stem Cells Dev.* 2012;21(12):2273-87.
41. Ghosheh N, Olsson B, Edsbagge J, Kuppers-Munther B, Van Giezen M, Asplund A, et al. Highly Synchronized Expression of Lineage-Specific Genes during In Vitro Hepatic Differentiation of Human Pluripotent Stem Cell Lines. *Stem Cells Int.* 2016;2016:8648356.
42. Siller R, Greenhough S, Naumovska E, and Sullivan GJ. Small-molecule-driven hepatocyte differentiation of human pluripotent stem cells. *Stem Cell Reports.* 2015;4(5):939-52.

43. de Villiers WJ, van der Westhuyzen DR, Coetzee GA, Henderson HE, and Marais AD. The apolipoprotein E2 (Arg145Cys) mutation causes autosomal dominant type III hyperlipoproteinemia with incomplete penetrance. *Arterioscler Thromb Vasc Biol.* 1997;17(5):865-72.
44. Sullivan PM, Mezdour H, Quarfordt SH, and Maeda N. Type III hyperlipoproteinemia and spontaneous atherosclerosis in mice resulting from gene replacement of mouse Apoe with human Apoe*2. *J Clin Invest.* 1998;102(1):130-5.
45. Huang Y, Schwendner SW, Rall SC, Jr., and Mahley RW. Hypolipidemic and hyperlipidemic phenotypes in transgenic mice expressing human apolipoprotein E2. *J Biol Chem.* 1996;271(46):29146-51.
46. Backstrom JR, Sheng J, Wang MC, Bernardo-Colón A, and Rex TS. Optimization of S. aureus dCas9 and CRISPRi Elements for a Single Adeno-Associated Virus that Targets an Endogenous Gene. *Mol Ther Methods Clin Dev.* 2020;19:139-48.
47. Brovkina AF, Sychev DA, and Toropova OS. [Influence of CYP3A4, CYP3A5, and NR3C1 genes polymorphism on the effectiveness of glucocorticoid therapy in patients with endocrine ophthalmopathy]. *Vestn Oftalmol.* 2020;136(6. Vyp. 2):125-32.
48. Constantinescu AE, Mitchell RE, Zheng J, Bull CJ, Timpson NJ, Amulic B, et al. A framework for research into continental ancestry groups of the UK Biobank. *Hum Genomics.* 2022;16(1):3.
49. Russcher H, Smit P, van den Akker EL, van Rossum EF, Brinkmann AO, de Jong FH, et al. Two polymorphisms in the glucocorticoid receptor gene directly affect glucocorticoid-regulated gene expression. *J Clin Endocrinol Metab.* 2005;90(10):5804-10.
50. El-Fayoumi R, Hagras M, Abozenadaha A, Bawazir W, and Shinawi T. Association Between NR3C1 Gene Polymorphisms and Toxicity Induced by Glucocorticoids Therapy in Saudi Children with Acute Lymphoblastic Leukemia. *Asian Pac J Cancer Prev.* 2018;19(5):1415-23.
51. Roerink SH, Wagenmakers MA, Smit JW, van Rossum EF, Netea-Maier RT, Plantinga TS, et al. Glucocorticoid receptor polymorphisms modulate cardiometabolic risk factors in patients in long-term remission of Cushing's syndrome. *Endocrine.* 2016;53(1):63-70.
52. Quax RA, Koper JW, Huisman AM, Weel A, Hazes JM, Lamberts SW, et al. Polymorphisms in the glucocorticoid receptor gene and in the glucocorticoid-induced transcript 1 gene are associated with disease activity and response to glucocorticoid bridging therapy in rheumatoid arthritis. *Rheumatol Int.* 2015;35(8):1325-33.
53. Bouma EM, Riese H, Nolte IM, Oosterom E, Verhulst FC, Ormel J, et al. No associations between single nucleotide polymorphisms in corticoid receptor genes and heart rate and cortisol responses to a standardized social stress test in adolescents: the TRAILS study. *Behav Genet.* 2011;41(2):253-61.
54. Durumutla HB, Prabakaran A, El Abdellaoui Soussi F, Akinborewa O, Latimer H, McFarland K, et al. Glucocorticoid chrono-pharmacology promotes glucose metabolism in heart through a cardiomyocyte-autonomous transactivation program. *JCI Insight.* 2024.
55. Prabakaran AD, McFarland K, Miz K, Durumutla HB, Piczer K, El Abdellaoui Soussi F, et al. Intermittent glucocorticoid treatment improves muscle metabolism via the PGC1alpha/Lipin1 axis in an aging-related sarcopenia model. *J Clin Invest.* 2024;134(11).
56. Chang CC, Chow CC, Tellier LC, Vattikuti S, Purcell SM, and Lee JJ. Second-generation PLINK: rising to the challenge of larger and richer datasets. *Gigascience.* 2015;4:7.